END
DATE
FILMED
3 - 78
DDC

MICROCOPY RESOLUTION TEST CHART

NATIONAL BUREAU OF STANDARDS-1963-A

AUDIBLE AND ULTRASONIC ACOUSTIC EMISSIONS FROM

COMPOSITE SOLID PROPELLANTS

Prepared for

Air Force Office of Scientific Research/NA
Bolling Air Force Base, D. C. 20332

by

William A. Bell
James I. Craig
Warren C. Strahle

School of Aerospace Engineering
Georgia Institute of Technology
Atlanta, Georgia 30332

Approved for public release; distribution unlimited

<u>Conditions of Reproduction</u>

AFOSR FINAL SCIENTIFIC REPORT

(6) AUDIBLE AND ULTRASONIC ACOUSTIC EMISSIONS FROM

COMPOSITE SOLID PROPELLANTS,

Prepared for

Air Force Office of Scientific Research/NA
Bolling Air Force Base, D. C. 20332

(9) Final rept. Oct 76 - Sep 77,

by

(10) William A. Bell,
James I. Craig,
Warren C. Strahle

(16) 2308   (17) A1

School of Aerospace Engineering
Georgia Institute of Technology
Atlanta, Georgia 30332

(18) AFOSR (19) 78-0449

DDC
RECEIVED
FEB 2 1978
B

(12) 69 p.

(15) Approved for public release; distribution unlimited

Grant No. AFOSR-75-2805

(11) Sep 77

Conditions of Reproduction

403 914

Abstract

The audible and ultrasonic acoustic emissions from deflagrating composite solid propellants were monitored and analyzed to evaluate their potential use as diagnostics of the combustion and as a means for the study of fundamental burning processes. A family of composite HTPB-AP propellants were tested which include a range of AP particle sizes, aluminized and nonaluminized formulations, the effect of the additon of a catalyst, and the presence of an AFCAM aluminum coating.

For the audible emissions, the frequency behavior in the 0-10 kHz range can be explained by assuming the gas phase reaction time primarily controls the oscillating frequency. The combustion noise efficiency, η, cannot be explained by the theories put forth, so the physical makeup of the noise source is presently unknown.

Analysis of the ultrasonic emission spectra indicates that there are no distinct spectral features which can be used to identify a particular propellant by its acoustic signature. The rms emission levels, however, can be used as a reliable, non-intrusive means for detecting flaws in the propellant, identifying bad burns, and measuring burn rates. The overall level increases with increasing burn rate and chamber pressure and decreasing particle size.

ACCESSION for

NTIS	White Section ☑
DDC	Buff Section ☐
UNANNOUNCED	☐
JUSTIFICATION	

BY

DISTRIBUTION/AVAILABILITY CODES

Dist.	AVAIL. and/or SPECIAL	
A		

Table of Contents

I. Introduction

Deflagration of composite solid propellants is a complex, unsteady process involving a heterogeneous material. Consequently, experimental studies of the combustion dynamics are difficult to perform because of both the inaccessability of the process and the relatively small scale of heterogeneities. Average or integrated properties, such as the burn rate or the characteristic acoustic impedances of the propellant surface, have been measured during deflagration; but the details of the combustion processes must generally be studied by microscopic examination of the quenched propellant surface.

To study the dynamics of localized combustion phenomena, motion pictures using high speed cameras and photographs of the burning propellant surface are often used. With these visual aids phenomena such as binder melts and, with metallized propellants, the formation and burning of the metal particles have been studied. However, the microscopic surface details tend to be obscured by the flame front, smoke, and metal particles.

To augment the visual studies the investigation reported here is concerned with the use of audible and ultrasonic acoustic waves generated during deflagration to assist in the analysis of the combustion dynamics. These emissions are a direct result of unsteadiness caused by the heterogeneity of the propellant, and their measurement exemplifies the use of acoustic analysis in "turbulence" diagnostics. This technique consists of analyzing the frequency spectra of the noise produced by the deflagrating solid propellant and relating the spectral characteristics to specific combustion processes. Deduced free field audible emission measurements were taken and cover a range of frequencies from 40 Hz to 10 kHz. Using combustion noise scaling laws[1-3], the objectives of the audible emission studies are to (1) relate the frequency spectra of the emissions to known propellant properties and (2) determine from overall sound power level the mass flow noise efficiency (acoustic power output per unit mass flow rate). The ultrasonic emissions

(sometimes referred to as acoustic emissions) were also measured and reliable data obtained from 50 kHz to 300 kHz. Recent studies of deflagrating solid propellants[4,5] have attempted to relate variations in acoustic emission levels to instantaneous variations in burn rate. The objectives of the ultrasonic emissions studies reported here are to (1) relate the spectral features to the combustion dynamics and (2) determine the feasibility of using the overall ultrasonic sound power level in both steady and unsteady deflagration diagnostics.

The acoustic fields for a family of AP-HPTB composite propellants, including coated and uncoated aluminized as well as nonaluminized formulations, were analyzed. The AP particle sizes range from 0.5 to 400 microns, and the propellants were burned in helium, air, and N_2 at pressures of from 5 to 30 ATM.

Acoustic data showing the effects of presurization gas, AP particle size, aluminum addition, aluminium coating, and pressure are presented and discussed. The empirical mass flow noise efficiencies and half-power frequencies for the audible emissions are correlated with physical properties of the propellant to obtain scaling laws which are then compared with theory. In the ultrasonic emission studies, both power spectral and rms amplitude data are used to deduce information concerning the combustion dynamics.

II. Experiment

The deflagration tube shown in Fig. 1 is used in this study and can operate at pressures up to 70 Atm. The tube consists of a stainless steel pipe 162.5 cm in length with a nominal ID of 10.16 cm and an O.D. of 15.25 cm. The tube dimensions were originally chosen to satisfy the following criteria: (1) the volume of the tube should be sufficient so that the mean pressure level does not increase more than 10% during a run for the propellant strands used in this study; (2) the tube should be long enough to ensure fully developed wave propagation at some axial distance sufficiently far from the propellant; and (3) the first transverse mode should have a frequency higher than that expected for the peak of the sound power spectrum emitted from the propellants. Recent developments in accounting for three-dimensional waves in the tube have made it possible to relax this last assumption. Provisions are made along the tube for pressurization and evacuation. The gases used in this study were nitrogen, air, and helium.

At one end of the tube, the solid propellant sample is held with epoxy to an aluminum sample holder which is bolted to a steel endplate 2.5 cm thick. Behind this endplate, directly opposite the sample, a Dunegan-Endevco Model D 9201 flat response transducer is mounted to measure the ultrasonic acoustic emissions. To ensure a clean transmission path for the signal, high-vacuum grease is used between the sample holder and the endplate and a coupling grease is employed at the transducer-endplate interface. Electrical connections on the endplate allow the ignition wire to be joined to the igniter.

At the other end of the tube is another endplate to which a rupture disc is attached, as shown in Fig. 1. Twenty centimeters away along the axis of the tube a termination disc is located with a vent hole in the center. Fiberglass is placed between the disc and the endplate acts as a Helmholtz resonator and reduces the high amplitudes which occur at the lower resonant frequencies of the

tube so that better signal resolution can be achieved at the higher frequencies. Directly in front of the termination disc, the audible transducer - a BBN Model 376A piezoelectric sensor - is located. To minimize pressure differentials across the transducer, it is surrounded by a cylindrical cavity which is coupled to the deflagration tube.

As shown in Fig. 2, the signals from both the audible and ultrasonic transducers are amplified, filtered, and then recorded on an Ampex 14-channel tape recorder at a speed of 60 inches per second. The FM mode is used for the audible signals and the AM mode is selected for the ultrasonic signals. The upper limit of response for the tape recorder is 300 kHz. The signals are then played back at a reduced rate for digital Fourier analysis using an HP5451A Fourier Analyzer. Typical results are presented in Fig. 3 for the audible signal and consist of the power spectrum over a specified frequency range. The narrow peaks occur at the resonant frequencies of the tube. A theory has been developed to deduce the equivalent free field spectra from the tube spectra and is presented in the next section.

III. Theory

<u>Audible Theory - Propellant in Tube</u>

Consider Fig. 4 where a heterogeneous solid propellant is located in the acoustic tube with the propellant surface at the end plate position, $x = 0$. Because of the propellant heterogeneity, the axial velocity profile will be spatially nonuniform. Moreover, at a fixed space location the velocity will be nonuniform in time due to alternate burnthrough of particles. The "frequency" of the fluctuating velocity is expected to be $\theta(\dot{r}/l_p)$. Typically, for $\dot{r} = 0.5$ in/sec and $l_p = 100 \mu m$ $\nu \approx 130$ Hz. The fuel and oxidizer gases mix and react as they travel downstream and the initial velocity profile becomes smoothed as shown in Fig. 4. A typical dimension for this is of the order of hundreds of μm. However, after smoothing, there is still a temporal fluctuation in the axial velocity because the spacewise average mass flow is nonuniform, due to the heterogeneity of the propellant. This fluctuation in the space averaged axial velocity is the source of the acoustic signal.

Consider a sample with $d_p \gg d_R$ so that the mixing layer has penetrated the propellant gas stream a negligible amount by the time the smoothed velocity profile is achieved. Furthermore, for $d_R \ll \lambda$, as is the case under consideration, the smoothed profile may be considered at $x = 0$ for purposes of acoustic calculations. At $x = d_R$ there will also be spacewise and timewise fluctuations in density because of the space and timewise local mixture ratio fluctuations. The significance of $x = d_R$ is that fluctuations have become small compared with mean values so that small disturbance theory may be used.

It will now be assumed that the propellant properties and solid temperature are such that the mean speed of sound is the gases at $x = d_R$ is equal to that of the tube pressurization gas. This is generally not the case but simplifies the analysis, and a correction will be applied to the results after the analysis

is complete.

Assuming the gas velocity to be primarily axial, the region between $x = 0$ and d_R may be treated in a quasi-steady manner (mass flow in = mass flow out) if $\omega\, d_R/\bar{u} \ll 1$. For $d_R = 500\,\mu$m and $\bar{u} = 50$ ft/sec, $\omega\, d_R/\bar{u} \approx 0.02$ for the frequency cited above. Consequently, applying small perturbations to the mass flow per unit area

$$\frac{m'}{\bar{m}} = \frac{\rho'}{\bar{\rho}} + \frac{u'}{\bar{u}} \quad \text{or} \quad \frac{m_\omega}{\bar{m}} = \frac{\rho_\omega}{\bar{\rho}} + \frac{u_\omega}{\bar{u}} \tag{1}$$

This quantity may be locally calculated at $x = d_R$, and the average over the gas flow area must equal the total mass flux fluctuation at the propellant surface.

Assuming perfect gases, the density fluctuation may be written as an isentropic part plus an entropy fluctuation. In transform space this is

$$\frac{\rho_\omega}{\bar{\rho}} = \frac{1}{\gamma} \frac{p_\omega}{\bar{p}} + \sigma_\omega \tag{2}$$

Combination of Eqs. (1) and (2) yields

$$\frac{u_\omega}{\bar{u}} = \frac{m_\omega}{\bar{m}} - \frac{1}{\gamma} \frac{p_\omega}{\bar{p}} - \sigma_\omega \tag{3}$$

It is well known that $\bar{p}$ is constant to terms of the order of the square of a typical Mach number compared to unity. Moreover, in acoustics, flow effects only enter to terms of the order of the Mach number compared with unity. Since typical Mach numbers for solid propellant gases are approximately 0.01, small Mach number approximations will be valid. Care must be taken here, however, because flow effects are the cause of the emitted sound.

The tube acoustics will obey the Helmholtz equation for the transform of

pressure

$$\nabla^2 p_\omega + k^2 \, p_\omega = 0 \qquad (4)$$

The boundary conditions will assume that the tube side wall is hard and the end plate at $x = 1$ is characterized by a specific acoustic admittance. These boundary conditions are therefore

$$\left. \frac{\partial p_\omega}{\partial r} \right)_{x,a,\theta} = 0$$

$$\left. \frac{\partial p_\omega}{\partial x} \right)_{1,r,\theta} + i \, k \, \beta \, p_\omega(1,r,\theta) = 0 \qquad (5)$$

Eqs. (4) and (5) are homogeneous; the forced oscillation will arise from an inhomogeneous boundary condition at $x = 0$.

The boundary condition at $x = 0$ consists of $\partial p_\omega / \partial x = 0$ over all of the tube wall excluding linearized, transformed continuity and axial momentum equations near $x = d_R \approx 0$.

$$i \, \omega \, \rho_\omega + \bar{\rho} \, \nabla \cdot \underset{\rightarrow}{v}_\omega + \bar{u} \, \frac{\partial p_\omega}{\partial x} = 0 \qquad (6)$$

$$i \, \omega \, \bar{\rho} \, u_\omega + \bar{\rho} \, \bar{u} \, \frac{\partial}{\partial x} \, u_\omega = - \, \frac{\partial p_\omega}{\partial x} \qquad (7)$$

Combining Eqs. (2), (3), (6) and (7), there results

$$- \frac{1}{\bar{p}} \, \frac{\partial p\omega}{\partial x} = \gamma \, \bar{M} \left[- \frac{2ik}{\gamma} \left(\frac{p_\omega}{\gamma \bar{p}} + \sigma_\omega \right) + ik \, \frac{m_\omega}{\bar{m}} - \frac{1}{c} \, \nabla_{r,\theta} \cdot \underset{\rightarrow}{v}_{\omega a} \right] \qquad (8)$$

where terms of $\theta(\bar{M}^2)$ compared with unity have been neglected. Moreover, the first and last terms on the right hand side of Eq.(8) may be neglected as being of $\theta(\bar{M})$ compared with unity. There results as the boundary condition

at $x = 0$,

$$\frac{\partial p_\omega}{\partial x}\bigg)_{0,r,\theta} = 0 \quad \text{off of } S_p$$

$$\frac{\partial p_\omega}{\partial x}\bigg)_{0,r,\theta} = -ik\bar{p}\,\gamma M\left[\frac{m_\omega}{\bar{m}} - 2\sigma_\omega\right]$$

$$\equiv -D_\omega\,ik\bar{p} \tag{9}$$

where D_ω is the transform of the complicated acoustic source. It is D_ω that is to be measured in the experiments. On the right hand side of Eq. (9) an $\bar{M}$ multiplies the source terms. This cannot be neglected precisely because it is the acoustic source. Previous neglect of terms of the order of $\bar{M}$ compared to unity only was made when derived quantities were being compared, not source quantities.

The solution to Eq. (4) subject to Eqs. (5) and (9) follows by standard acoustics methods.[6,7,8] It is, when evaluated at $x = \ell$, $r = a$ and $\theta = \tilde{\theta}$,

$$P_\omega(\ell, a, \tilde{\theta}) = \sum_{\substack{m,n=0 \\ \sigma = \pm 1}}^{\infty} \frac{\Psi_{mn}^\sigma(a, \tilde{\theta})}{i\,k_{mn}\,\Lambda_{mn}} \frac{F_{mn}(\ell)}{S}$$

$$\Psi_{mn}^\sigma = J_m(\varkappa_{mn}a) \begin{Bmatrix} \cos m\tilde{\theta} \\ \sin m\tilde{\theta} \end{Bmatrix} \quad \begin{matrix} \sigma = +1 \\ \sigma = -1 \end{matrix}$$

$$k_{mn}^2 = k^2 - \varkappa_{mn}^2 \qquad \varkappa_{mn}J_m'(\varkappa_{mn}a) = 0$$

$$\Lambda_{mn} = \frac{1}{\varepsilon_m}\left[1 - \frac{m^2}{(\varkappa_{mn}a)^2}\right]J_m^2(\varkappa_{mn}a) \qquad \begin{matrix} \varepsilon_0 = 1 \\ \varepsilon_m = 2 \quad m > 0 \end{matrix}$$

$$F_{mn} = + \frac{i k \bar{p}}{k}\frac{\delta_\omega\,S_p}{\frac{k}{\bar{k}_{mn}}\beta_{mn}\cos k_{mn}\ell + i\sin k_{mn}\ell}$$

$$\delta_\omega = \frac{1}{S_p}\int_{S_p} D_\omega\,\Psi_{mn}^\sigma(r,\theta)\,dS \tag{10}$$

Equations (10) show the familiar phenomenon of cut-off whereby at sufficiently low frequency the transverse modes are not propagational. In such a case the plane wave mode is dominant and the solution simplifies to

$$k = k_{oo} \qquad \mathcal{K}_{oo} \approx 0$$

$$P_\omega(\ell) = \frac{\bar{P}}{S} \frac{S_p \int D_\omega \, dS}{\beta_{oo} \cos k\ell + i \sin k\ell} \tag{11}$$

It is also to be noted that in the experiment $S_p \ll S$ and the propellant is on the axis. Since $\Psi_{mn}^\sigma (0,\theta) = 0$ for $m \neq 0$, only the symmetric transverse modes will be substantially excited. This will justify a later experimental procedure of only accounting for the plane and purely radial modes of the tube. Since $\Psi_{o,n} (0,\theta) = 1$, $\delta_\omega \approx S_p \int D_\omega \, dS$ for all modes.

In Eq. (11) resonances can clearly be identified near $\sin k\ell = 0$ as shown in Fig. 3. Note, however, that near minima $\cos k\ell \approx 0$, and the result is independent of β_{oo}. This is used to advantage in the data reduction procedure. From Fig. 3 if a line is drawn connecting the minima in the power spectrum, then the amplitude of the source term at a given frequency is

$$\delta_\omega \approx \int_{S_p} D_\omega \, dS = \frac{S \, P_\omega(\ell)_{min}}{\bar{P}}$$

Thus, the envelope formed by the line drawn through the minima represents the deduced power spectrum of the propellant in the absence of tube effects.

To correct for the speed of sound effect, for propellants which have their gas phase speed of sound different from the tube pressurization gas speed of sound, note that Eq. (9) is valid with k based upon the propellant gas speed of sound. In the limit that the propellant shrinks to a point source, Eq. (4) subject to Eqs. (5) and (9) is still the appropriate acoustics problem

but with k in Eq. (4) based upon the pressurization gas speed of sound. Tracing through the solution the net effect is to place a factor of $\bar{c}/\tilde{c}_p$ in the right hand side of Eq. (11). Then constructing the one sided spectral density of the pressure,

$$G_p = \frac{S_p^2 \bar{p}^2 \bar{c}^2 G_\delta}{S^2 c_p^2 \left[\sin^2 k\ell + \beta_{oo}^2 \cos^2 k\ell + \beta_{oo} i \sin 2k\ell \right]}$$ (12)

is the formula used in the data reduction procedure when only the plane wave mode is present. It will later be seen that a quantity which is a property of the propellant alone is $\hat{G}_\delta = S_p G_\delta$, and this will be used in what follows.

Audible Theory - Propellant in Free Space

Another way to present the data is to present an acoustic efficiency when radiating to free space. This is the method often used for other flame noise radiation studies. If the flame were radiating to free space and the source dimension is small compared with a wavelength, the solution at distances far from the source is

$$P_\omega = \frac{e^{-ikr}}{4\pi r} \quad i \frac{\omega}{\tilde{c}_p} \bar{p} \int_{S_p} D_\omega dS$$

with a one sided spectral density given by

$$G_p = \frac{1}{(4\pi r)^2} \left(\frac{\omega}{\tilde{c}_p} \right)^2 \bar{p}^2 \, S_p \hat{G}_\delta$$ (13)

The mean square value of the acoustic pressure is

$$<p'2> = \int_0^\infty G_p \, d\omega$$

and the acoustic power is

$$P = 4\pi r^2 \frac{<p'2>}{\bar{\rho} \, \bar{c}}$$

An acoustic efficiency is defined as

$$\eta = P/\dot{m} \; \dot{r}^2 \tag{14}$$

which is also used in the data reduction. $\hat{G}_\delta$ is determined from experiment and Eq. (11), and Eqs. (12) and (13) are used to construct the free space radiation properties.

Ultrasonic Theory

Acoustic emissions can be broadly defined as stress wave emissions propagating within a solid material in response to some type of loading. The emission levels are generally well below those associated with audible disturbances and for many materials are on the order of microbars.

The temporal characteristics of the emissions may range from continuous to pulsatile although a burst type activity is commonly observed in materials studies. From the earliest investigations into the acoustic emission phenomenon to the present (for summaries see Refs. (9,10)), attention has been directed primarily to the amplitude characteristics of basically impulsive signals. The most popular technique has been to use a piezoelectric ceramic disc encapsulated in an epoxy shoe. Each time an emission stress wave is received, a proportional electrical charge is produced on faces of the ceramic. Unfortunately, most elements exhibit strong mechanical resonances in the range from 100 kHz to 1 MHz and consequently the commonly observed electrical output is a ringing type response at one or more of these natural frequencies. This is satisfactory for event detection where frequency of occurence (and the location) of an event are of prime importance. The approach is also useful when an analysis of the emission energy per event is performed. On these grounds, acoustic emission analysis has been successfully employed for flaw location in pressure vessels and other structures, weld inspection, fatigue studies and fracture mechanics in metals and composite fibrous materials.

Deflagrating solid propellants produce much more of a uniform acoustic emission level with little pulsable behavior noted above. Consequently it is more useful to consider the emissions as realizations of a random process with energy distributed over a broad frequency band. The approach taken in the present study involved a combination of both spectral and temporal techniques best

suited to the continuous type acoustic emission signal observed during defla-
gration. The auto power spectrum provided the means to study the frequency
distribution of power in the signal. This type of analysis was performed on
digitized sample records of the recorded signal. In addition, an analog cir-
cuit was designed to provide a simultaneous rms acoustic emission signal
(averaging time adjustable) whose spectral content and temporal behavior
were analyzed.

Study of the ultrasonic emission spectrum must, at present, be general in
nature for basically three reasons. First, the general meaning of the spectrum
has yet to be formulated in any area of study. For solid propellants the in-
ability to precisely define the propellant acoustical properties and its in-
homogeneity greatly complicate data interpretation. Secondly, a suitable acous-
tic emission transducer with adequate bandwidth and relatively uniform response
above 100 kHz is unavailable. Finally, frequency dependent attenuation of the
waves caused by their dispersive propagation through the propellant and signal
distortion produced by reflection at interface complicates data interpretation.

To account for the lack of flat transducer response on the spectral analysis,
a transducer calibration spectrum was used to correct the measured spectra. At
the outset, a calibration curve determined by the manufacturer using an impul-
sive acoustic emission technique was used for this purpose. This curve shows a
smooth behavior from about 50 kHz to the 300 kHz limit of the tape recorder.

In order to provide finer spectrum detail, an alternate qualitative cali-
bration technique was used (Bell, Craig, Strahle). Instead of measuring the
transducer output for a known input stress wave (pressure), the electrical im-
pedance of the transducer was measured over the frequency range of interest.

Because of the reversible nature of the piezoelectric effect, the trans-
ducer's driven electrical impedance will generally show a strong qualitative

similarity to the actual stress wave calibration. The electrical impedance was measured for the as-mounted configuration and quantitatively matched at the peak response (near 100 kHz) to the absolute calibration wave furnished. The most notable difference was the presence of several small (1-3 dB) peaks near 180 kHz and above 300 kHz. Rolloff at 100 kHz for the "impulse" calibration reflects the rolloff of the preamp used by the manufacturer in this test.

The temporal characteristics are also affected by the nonhomogeneities and geometric irregularities in the transmission media. As a result, the received signal may bear little resemblance to the pressure wave produced at the emission source. Three mechanisms can be immediately noted:

(a) material dispersion in the viscoelastic, heterogeneous propellant

(b) geometric dispersion for a stress wave propagating in a prismatic bar

(c) attenuation due to acoustic impedance mismatch at material interfaces in the transmission path.

The first two are difficult to define quantitatively; however, qualitatively, geometric dispersion is most pronounced at wavelengths about equal to the corss-section dimensions of the propagation medium. Since the estimated wavelengths in the propellant at from 100 kHz to 1 MHz are much less than the typical strand cross sections used in the experiments, geometric dispersion should be small, but dispersion due to propagation through the heterogeneous material containing AP particles comparable in size to emission wavelengths will be larger.

Attenuation due to acoustic impedance mismatch will occur at the propellant-holder, the holder-end-plate, and the endplate-transducer interfaces (Figure 1). To a first approximation the overall attenuation for complex waves may be represented as:

$$\text{Attenuation} = \frac{2}{1 + \dfrac{\rho_2 c_2}{\rho_1 c_1}}$$

where ρ = density, d = wavespeed, and propagation is from 1 to 2. For the present experimental configuration, the net attenuation is approximately 0.0026 so that less than 1% of the energy at the source will arrive at the transducer element.

The temporal characteristics of the acoustic emissions were studied by analysis of the rms signal recorded simultaneously. Three aspects of the signal behavior can be examined in this way:

(a) Signal power as a function of burn time. During the deflagration, the propellant strand effective length is decreasing continuously so that the acoustic emission path length is changing accordingly. Changes in the rms level with time can therefore be related to attenuation characteristics or to burn rate effects.

(b) Propellant imperfections. Abrupt changes or irregular behavior in the rms signal are indicative of amomalies in the deflagration process. In the simplest arrangement, this can be used to determine burn times.

(c) Spectral properties. When the rms averaging time is adjusted to a sufficiently short period (less than the period of the highest frequencies of interest), it is possible to computed an auto power sepctrum for the rms signal.

The first technique can be used to determine the attenuation characteristics, and then in reverse, to estimate the emission source power as a function of propellant formulation and test conditions. The second technique has been employed by several groups (4,5) to determine the quality of a burn. The spectral properties of the rms signal can be computed over the audible range of frequencies by adjusting the rms averaging time to on the order of 100 measurements. In this way, a comparison between the audible and acoustic emissions can be

made. For example, if the acoustic emissions are affected by microscopic level changes in the burn rate, it would be anticipated that under conditions of strong feedback (eg. in a driven impedance tube or a "T" burner) peaks would appear in the rms spectra at the driving frequencies. On the other hand, if the audible emissions are largely the result of gas phase effects occuring at relatively large distances from the propellant surface, there would be little correlation with the rms acoustic emission spectra.

In order to provide a firmer basis for the exploratory work, several mechanisms were considered as potential sources for the measured emissions. They can be broadly grouped as:

(a) solid phase effects such as dislocation kinetics or crystal fracture,

(b) gas phase phenomena such as ignition transients or combustion kinetics. Since for these tests, energy has been analyzed over a 50 kHz to 300 kHz band, the sources can be further grouped according to characteristic frequencies. Solid phase effects are commonly observed as sources for acoustic emissions in materials tests, however, the characteristic times are in the sub-micro-second range so that the major energy release would occur well above the present band (and outside the range of all but the most exotic equipment). Furthermore, should this energy excite individual particles to vibrate, the characteristic frequencies (AP particles, for example) would again fall above 1MHz.

Chemical kinetics times, on the other hand, are typically on the order of 10 microseconds so that energy in the 50kHz to 1MHz range can be anticipated. Three potential mechanisms can be hypothesized:

(i) Laminar flame moving through a small volume of fuel immediately above an AP particle,

(ii) AP ignition transient as the gas above a particle igniter,

(iii) Explosive ignition of a fuel-oxidizer mixture near the surface.

While the characteristic times are all comparable, the resultant pressure disturbances can range from about 50 to 5000 microbar at the transducer for the first two cases, or in the third case to more than 1 bar.

These general observations have been systematically explored in the present study and the observations and conclusions are reported on in the following sections.

IV. Results and Discussion

Burn Rate

The physical properties of the propellants tested are presented in Table 1. These propellants are basically hydroxyl terminated polybutadine - ammonium perchlorate (AP) with and without aluminum (Al) and some additives. Parameter variations are systematically made in AP size, aluminum coating (AFCAM), catalyst and percentage of binder.

The burn rates for combustion in nitrogen and helium are shown in Table 2 at mean chamber pressures of from five to 30 Atm. For the MC propellant series a mass weighted average of the particle sizes was taken. Although no direct observation of the burn rate was possible, it was determined from the onset and termination of the ultrasonic signals. Assuming a power law dependence on binder ratio F, pressure, speed of sound in the tube, and AP diameter, the burn rate obtained by regression analysis using the data in Table 2 is

$$\dot{r} \sim F^{-.83} \ \bar{p}^{.5} \ c_t^{.15} \ D_{AP}^{-.26}$$

By analysis of the cross correlation coefficients, the burn rate is essentially independent of the tube speed of sound, as expected. To within the scatter in the experimental results, an AFCAM coating does not significantly affect the burn rate. Introduction of the catalysts increases the burn rate from 50 to 100 per cent.

From the regression analysis, the burn rate decreases with increasing binder ratio and AP size. Increasing the pressure increases the burn rate.

Experimental Results for Audible Emissions

The combustion noise efficiency and half power frequency for those propellants for which reliable emission data were obtained are presented in Table 2. Although considerable effort was made to ensure consistent sample preparation, large variations in the combustion noise efficiency are evident which makes data

interpretation qualitative at best. The efficiency is computed by integrating the audible spectrum over the frequency range from 40 to 1000 Hz. These parameters were also obtained from 40 to 10,000 Hz using the analysis given in Section III which accounts for the transverse modes existing in the tube above the cutoff frequency of 2000 Hz. For tests conducted in nitrogen the data indicate that most of the noise is produced at frequencies above this value as shown in Fig. 5. To isolate the tube effects from the propellant noise spectra, tests were conducted using helium rather than nitrogen as the wave propagation medium since the speed of sound is greater in helium by a factor of 2.88. Therefore, the cutoff frequency is increased from two to approximately six kiloHertz. From Fig. 5 the effect of helium is to shift the entire power curve to the right. This type of behavior would occur if (1) the noise from the propellant is dependent upon the tube speed of sound or (2) the propellant emits essentially white noise and the spectral features are entirely tube dependent. Regardless of the cause, the analysis in Section III can be used above the cutoff frequency to determine the deduced freefield spectra. However, above this frequency the data are considered qualitative since, in the theoretical analysis in Section III, the propellant combustion noise is assumed to arise from a point source at the center of the tube and at the position $x = 0$. In reality the combustion is distributed over a finite area, the sample length is finite and, because of localized combustion on the surface of the propellant sample, the source may not coincide exactly with the tube axis. Thus, tangential modes could be excited above the cutoff frequency, so the spectral details could be attributed to the cuton of tangential modes rather than deflagration behavior. Because of these uncertainties, the data is presented only over the range from 40 to 2000 Hertz and η and $\omega_{\frac{1}{2}}$ computed over the range from 40 to 1000 Hz.

The deduced free field spectra for the MC, NT, and T propellant series' are presented in Figs. 6, 7, and 8 respectively. Certain spectral features are common to each propellant. First there is an overall decrease in power level from 100 to approximately 1000 ± 200 Hz for the tests run in nitrogen. Upon reaching a minimum at 1000 Hz, the power level increases again from one to two kiloHertz. The cause of this behavior is not known and attempts to relate this phenomenon to the tube acoustics have been unsuccessful. Secondly, the tests performed in helium yield power levels approximately 10db lower than the nitrogen runs over the frequency range from 100 to 2000 Hz.

For the aluminized propellants, the effects of propellant properties and pressurization gas on the measured spectra are presented in Fig. 6. Comparison of the curves for MC-177 burned in air and nitrogen indicates a 10 to 15 db rise in sound power level for the run with air. The difference in the results appears to be caused by aluminum afterburning. The effect of an AFCAM coating can be observed from comparison of the spectra for MC-170 and 172. The propellant without AFCAM has a slightly higher noise output over the frequency range from 200 to 2000 Hz.

Also shown on Fig. 6 are the burn-through frequencies computed from $\nu = \dot{r}/D_{AP}$ using the MC-170 burn rate for various AP and Al particle sizes. Because of variations in granularity, it is seen that the spectrum is rather densely occupied by available frequencies. No apparent correlation of the observed spectra with these frequencies is evident - either from the figures or from the half-power frequencies presented in Table 2. None was really expected to be clear because of the roughness of the estimate of frequency, the usual spread of particle size about the stated value and the dense population of the spectrum with these particle frequencies. Also the frequencies for the 200 and 400 μ particle sizes are below the rolloff frequency of the transducer system. Moving from

MC-170 to MC-177, which increases the mean particle size and decreases the burn rate (see Tables 1 and 2), there is a general decrease in the spectral power level from 100 to 2000 Hz.

In contrast to the aluminized propellants, the spectra for the non-aluminized NT series propellants, shown in Fig. 7, indicates a general increase in noise with decreasing particle size over the 1000-2000 Hz range. Comparison of the curves show a general increase in the sound levels from 300 to 2000 Hz probably caused by the higher burn rate of NT-4. Below 300 Hz no general trend can be ascertained. From 40 to 1000 Hz $\omega_{\frac{1}{2}}$ increases noticeably with decreasing particle size for NT-2 and NT-3 in nitrogen. However, the shift in the half power frequency is not as large as expected.

For the T series non-aluminized propellants, no general trend can be determined concerning the variation in the spectra with particle size. The binder to oxidizer ratio does appear to have an influence. There is an increase in power level from the 273 to the 81 micron particle sizes, possibly due to the increase in burn rate. However, a decrease of five to 10db in power level occurs for the propellant with the 48 micron particle size which has the lowest burn rate because of its relatively high binder to oxidizer ratio.

Comparison of Theory and Experiment

Because of the lack of any marked change in the shape of the power spectra with propellant composition, a regression analysis was performed to determine the dependence of the combustion noise efficiency η and half-power frequency $\omega_{\frac{1}{2}}$ on (1) percentage of binder F, (2) chamber pressure, (3) tube speed of sound, (4) AP particle diameter, and (5) burn rate. Including the area of the propellant in this analysis shows that η and $\omega_{\frac{1}{2}}$ are independent of this parameter, which is consistent with previous results.[8] The results of the regression analysis are presented in Table 3 and the following empirical relations are obtained

from 0 to 1000 Hz.

$$\omega_{\frac{1}{2}} \sim F^{.38} \; \bar{P}^{.09} \; C^{-.49} \; D^{-.07} \; \dot{r}^{-.19}$$

$$\eta \sim F^{-.5} \; \bar{P}^{-1.9} \; C^{-1.4} \; D^{-.16} \; \dot{r}^{-1.5}$$

The correlation coefficients given in Table 3 are an indication of the inter-dependence of the dependent and independent variables. A coefficient which has a magnitude of unity indicates complete dependence, whereas a value of zero means no dependence whatsoever. For the half-power frequency, the only relatively strong correlation is with the speed of sound; and little correlation exists with the other variables. There is a strong correlation between η and $\bar{P}$, C, and r.

From the frequency spectra and the data of Table 3, the experimental frequency content shows the curious behavior that it is invariant with virtually any parameter. It was initially thought that the low frequency content (0-1000 Hz) would correlate with particle burnthrough times ($D/\dot{r}$), whereas the high frequency content would correlate with gas phase reaction times (τ_r). Clearly, however, the frequency content in both the high and low frequency regimes appears to be caused by the same mechanism. Allowing that another relevant time might be a molecular diffusion time ($\mu/\rho D^2 p = \tau_d$), it is tempting to attempt a correlation of the form

$$\omega_{\frac{1}{2}} = 1/(\tau_r^a \; \tau_b^b \; \tau_d^c)$$

with $a + b + c = 1$ to preserve dimensional homogeneity. The reaction time, if one assumes a global single-step equivalent reaction, would take the form

$$\tau_r = K \; F^m \; p^{1-n}$$

Here n is the effective overall order of the reaction and the F^m factor is empirical to take into account the fuel mass fraction effects and temperature

effects in the Arrhenius factor. It is expected that $m < 0$, since the propellants are fuel rich and an increase in F would lower the temperature and increase the reaction time. Since $\tau_d \propto 1/pD^2$ and $\tau_b = D/\dot{r}$, comparison with the 0 - 10,000 Hz empirical law from Table 3,

$$\omega_{\frac{1}{2}} \propto F^{.1} \, p^{-.1} \, c^{.2} \, D^o \, \dot{r}^{.1},$$

yields

$$a = .85 \quad b \approx .1 \quad c = .05 \quad m = 1.0 \quad n = 0.8$$

with similar results for 0 - 1000 Hz. These numbers are plausible, and, if the approach is correct, the frequency is primarily dependent upon the gas phase reaction time.

The empirical dependence upon the tube speed of sound may also be explained through the gas phase reaction time. Since the speed of sound was varied by using He instead of N2 as the pressurization gas and He has a very low molecular weight, the diffusion of He into the reaction zone may have affected the reaction rates.

All attempts at explaining the behavior of η have failed. At this time, therefore, the physical cause for makeup of the source term D_ω is unknown. Using an approach similar to that of Ref. 2, the η law may be coarsely explained by reasoning with Eq. (9). However, the agreement between theory and experiment is not as good as desired and those results will not be presented here.

Ultrasonic

Ultrasonic acoustic emission data were obtained for all propellants in Table 1 and consist of (1) power spectra and (2) rms amplitude plots taken during the course of the burn. In an effort to determine a relation between the physical properties of the propellant and the spectral features, the effect of the following variables on the spectral data are investigated: (1) AP particle size,

(2) pressurization gas, (3) aluminum particles, (4) AFCAM coating, and (5) catalyst. In addition, the chamber pressure was varied from 20 to 50 Atm, and the corresponding spectra were studied to gain insight into the nature of the source characteristics. The details of the data reduction methods are given in Ref. 6.

While a satisfactory explanation for the emission power spectra has not been formulated in all cases, there are nonetheless certain features that are present in all spectra regardless of the propellant type. During the ignition and burnout transients, the emission level is abnormally high and the spectra considerably distorted. In between, the signal exhibits stationary properties and an ensemble averaged estimate of the power spectrum can be calculated. Figures 9 through 13 show power spectra computed this way using from 260 to 1000 averages each. Each spectrum is characterized by large power around 100 kHz with secondary peaks between 175 and 200 kHz. The secondary peak was also observed in an earlier study[4] at Princeton at pressures on order of magnitude higher than for the present work. In almost every test to date, a mild nonstationary character was observed in the spectrum with the noise power over the 200-300 kHz range smoothly increasing during the course of the burn as shown in Fig. 14. This behavior is most likely due to the dispersive attenuation of the stress waves as they pass through a decreasing length of propellant before arriving at the transducer.

In general agreement with the Princeton work, the ultrasonic emission power spectra when corrected for background noise and transducer response tend to exhibit no readily distinguishable features which could be used to recognize a particular propellant. A more detailed discussion for each property considered follows:

AP Particle Size. For the nonaluminized propellants AP particle size has little effect on either the overall sound power level or the location of the peaks in the spectrum as shown in Fig. 9. Based on these data no correlation appears to exist between the spectral peaks and the particle size. Since in the T series propellants the particle sizes and mixing were carefully controlled to ensure uniformity of size and distribution, the lack of any pronounced effect on the spectra cannot be attributed to nonuniformities in propellant preparation.

Effect of Pressurization Gas. The burning of MC-177 in air as opposed to nitrogen products a definite shift in both spectral peaks and peak power as shown in Fig. 10. In air there is a stronger high frequency content than in nitrogen. There is also a general smoothing of the spectra for air at the frequencies below 125 kHz. These effects are most probably caused by aluminum afterburning although correlation between the spectral peaks and the combustion process is presently not clear.

Aluminum Particle Addition. As shown in Fig. 9, AP particle size does not have a pronounced effect on the spectra of the acoustic emissions. However, the addition of aluminum does. Comparison of the spectra for aluminized (MC-177) and nonaluminized (NT-2) propellants in Fig. 11 indicate markedly different spectral features. The spectrum of the aluminumized propellant has a large noise content at the low frequency range below 125 kHz. Also, the peaks in the aluminized propellant spectrum are more distinct in the 125 to 225 kHz range. Above 225 kHz. however, relatively little difference is apparent in the two spectra. Whether the cause of the differences is the emission source itself or propagation of the ultrasonic waves through the aluminized nonaluminized propellant cannot be ascertained.

Effect of AFCAM Coating. As reported in Ref. 6 there was a general increase in overall sound power when the aluminum is coated with AFCAM for MC-177 and MC-178. This trend is not exhibited for MC-170 and MC-172 as shown in Fig. 12, although the spectral peaks are different.

Effect of a Catalyst. In Fig. 13 catalyzed MC-173 and MC-179 propellants are compared to an uncatalyzed MC-170. The most distinct effects of a catalyst are evident in the overall sound power level and relative noise content.

Variation of the Spectra during Deflagration

Typical variations in the spectra taken at different times during a burn are shown in Fig. 14 for MC-170. The two most noticeable differences with time are relatively high acoustic emission levels below 100 kHz during ignition and a relative increase in noise content at the higher frequencies with increasing time. This trend is shown quantitatively by the shift to higher values in half-power frequency as the burn progresses. General spectral features, however, remain essentially unchanged from 100 to 300 kHz. The broad peak about 125 kHz and the secondary peak between 175 and 200 kHz are evident throughout the burn.

Effect of Chamber Pressure on the Acoustic Emission Spectra

The effect of increasing the chamber pressure is to increase the overall sound power levels as shown in Fig. 15. However, no marked change in the spectral features is observed for either the aluminized or non-aluminized propellant.

Source Characteristics. Based on the earlier observations reported in Ref. 6, it was strongly suspected that the AP deflagration mechanism was primarily responsible for the observed emission spectra. The consideration summarized in Section III of this paper provide a crude theoretical basis for this hypothesis as well. The rms acoustic emission levels at the transducer consistently range between about 800 to 3500 μ Bar. These levels are somewhat above the range for

the laminar flame model but are generally consistent with the AP ignition transient model. The chemical kinetics times associated with both of these processes are on the order of 10^{-5} sec so that the accompanying unsteady pressures would be expected to show relatively larger spectral energy content near 100 kHz. Again, this is consistent with the earlier observations of a large peak in the emission power spectra around 100 kHz. Furthermore, since these characteristic times should be only weakly affected by pressure and unaffected by AP size, the principal alteration in the emission spectra should be a change in the relative height of the 100 kHz peak as AP sizes and burn rates are varied. In this case, the change in level is associated with the changing source areas.

Unfortunately, as shown in Fig. 9, there is no clear difference in the shape or level of the emission spectra as the AP size is varied from 50 μ to 200 μ (NT series) although the level of the spectra increases in the 100 - 300 kHz range for the T series as the particle size decreases. The spectra show some fine structure but are basically flat within the tolerance of the calibration curve used. On the other hand, as shown in Fig. 11, it is much more likely that the observed peak at 100 kHz can be attributed to the Al present in the more complex MC propellants. This possibility has not yet been fully explored in tests to date, although several comments might be made. From the levels involved, the signals would likely be produced before the Al agglomerates have left the burning surface (there is some indication, however, that the peak may be due to Al particle impact on the inner tube wall, although a neoprene rubber sheet is used to line the tube and minimize this effect.) Emissions from the solid phase Al due to dislocation activity or micro-fracture are well above the 100 kHz range. Propellants with a range of Al sizes and quantities will have to be tested in order to further clarify these observations. For example, insensitivity to Al size could indicate a

source mechanism associated with the agglomerate phase.

In addition to spectral analysis, the rms levels of the ultrasonic emissions have also been obtained. In Fig. 16, a comparison between the rms level of tests conducted with NT-2 is presented. During one of the tests the burn rate of the NT-2 was abnormally high. The corresponding ultrasonic emission levels are significantly higher and exhibit much greater variations with time than the propellant with the low burn rate. These data are in agreement with the observations reported in Ref. 5 in a similar study conducted at Princeton. The Princeton group found that, for propellants with abnormally large mean burn rate deviations, an increase in both the level and unsteadiness of the acoustic emissions was observed. They conclude that such information can be of use in diagnosing the quality of the burning and, thus, of the propellants.

To confirm these conclusions, the behavior of the rms levels was investigated in the present study. To systematically evaluate the use of the emission levels as a diagnostic aid, three tests were conducted with MC-177 with flaws intentionally added. The first consisted of a half-inch slit in the center of the propellant parallel to the centerline of a $\frac{1}{4}$" by $\frac{1}{4}$" strand. The next flaw consisted of a 1/16" - diameter hole drilled through the center of the strand perpendicular to the centerline. In the last test two such holes were drilled one inch apart. The results of these tests are presented in Fig. 17. In all three tests the presence of the flaws are characterized by an abrupt increase in the rms levels. The large amplitude at the initiation of the burns is attributed to the igniter paste and typically lasts for approximately one second. The large increase in amplitude at the termination of the burns is caused by the burning of the epoxy which holds the propellant strand to the mounting plate.

These anomalous fluctuations in the rms levels were also observed in the nonaluminized propellants as shown in Fig. 18 for T-81. Upon examination of

the propellant, spherical cavities caused by bubbles in the manufacture of the propellant were observed and are probably responsible for the sharp increase in rms level which occur at various times during the burn. It appears, then, that the ultrasonic rms emission can be used to reliably detect irregularties in the propellant.

As shown in Figs. 19 and 20 the rms levels strongly depend upon the chamber pressure over the range from 5 to 30 Atm and the particle size. The general increase in the rms acoustic emission levels with chamber pressure shown in Fig. 19 may be caused by the alteration of the combustion zone and/or the increasing burn rate. In Fig. 20 the rms levels are seen to be definitely dependent upon AP particle size and increase in magnitude with decreasing size. Although the burn rate decreases for the 48 micron particle size because of a large binder percentage (30% vs. 15% for T-273 and 16.9% for T-81), the acoustic emission level is the highest. Thus, in addition to the level being a function of burn rate, as reported in Ref. 5, it is also a strong function of AP particle size.

In the final study conducted under this contract, a coherence analysis was performed between the audible signal and the rms fluctuations of the acoustic emissions. The results are shown in Fig. 21 for MC-170. Two hundred samples were taken over the course of the burn and the spectral averages of the audible and ultrasonic signals are presented. Although the rms fluctuations are on the same time scale as the audible signal, the coherence between the two is statistically insignificant.

V. Conclusions

Audible Emissions

1. The source of the audible output in the range 0-1000 Hz is presently unknown. Theories are presented to explain the behavior of the frequency and noise emission levels. The frequency appears to be primarily dependent on the gas phase reaction time; however, all attempts to explain the behavior of the combustion noise efficiency have been somewhat unsuccessful.

2. The strength of the audible signal is insufficient to account for the roughness levels in the rocket motor chamber pressure observed in practice. Therefore, some other causes must be responsible.

3. The main frequency content of the audible output appears to be between 3-10 kHz in nitrogen, and the signal is not altered by the variables investigated in the lower frequency range. It is currently conjectured that gas phase kinetic phenomena are responsible, but the high frequency content does not appear useful for combustion diagnostics.

Ultrasonic Signal

1. The ultrasonic spectra in the range 50-300 kHz are insensitive to propellant variables and are relatively flat. Overall emission spectral features are not sufficiently distinct to identify either a propellant or its deflagration characteristics from its acoustic signature alone.

2. The rms ultrasonic emission signal is a useful indicator of propellant flaws, bad burns, and propellant burn times. It is also a function of chamber pressure and AP particle size. Increasing the pressure and decreasing the particle size increases the rms signal.

3. The rms signal fluctuates on the time scale of the audible signal but is found incoherent with the audible signal. While it is suspected that both signals are causally related through the burn rate, the complex propagation path of the ultrasonic signal probably destroys phase coherence.

While the general tone of the conclusions appears negative, it must be pointed out that spectral analysis of acoustic emission signals in many other fields has been notably unsuccessful. The work reported here has improved the measurement techniques over previous studies, primarily by simplifying the transmission path from propellant to transducer response. In the time domain, the rms emission levels can be used to accurately measure burn times and to detect irregularities in the delfagration. It now appears that features in the rms signal may prove of more value as a diagnostic tool.

VI. Nomenclature

c	speed of sound
D	source function defined by Eq. (9)
d_p	width of propellant sample
d_R	length of gas phase reaction and mixing zone
G	one sided spectral density
k	wavenumber
ℓ	tube length
ℓ_p	mean particle size
M	Mach number
$\dot{m}$	total mass flow rate
m	mass flow rate/unit area
p	pressure
r	radial coordinate
$\dot{r}$	burn rate
S	tube area
S_p	propellant area
S_{cor}	area of correlated elements on the propellant surface
u	axial velocity
$\vec{v}$	vector velocity
x	axial distance
β	dimensionless specific acoustic admittance
γ	ratio of specific heats
δ	source function, $\int_{S_p} D\, dS$

η	acoustic efficiency
θ	angular coordinate
$\varkappa$	eigenvalue
λ	wavelength
ν	frequency
ρ	density
σ	entropy fluctuation
Ψ	eigenfunction
ω	angular frequency
$\nabla_{r,\theta}$	"del" operator in r and θ directions
$<\ >$	time mean operation

Superscripts

$'$	perturbation quantity
$-$	mean quantity

Subscripts

a	acoustic or dilatational part
mn	mn^{th} mode
p	pertaining to pressure or propellant gases
v	vortical or rotational part
δ	pertaining to δ
ω	Fourier transform

VII. References

1. Strahle, W. C., "Some Results in Combustion Generated Noise," Journal of Sound and Vibration, 23, 113-125, 1972.

2. Strahle, W. C. and Shivashankara, B. N., "A Rational Correlation of Combustion Noise Results from Open Turbulent Premixed Flames," Fifteenth Symposium (International) on Combustion, The Combustion Institute, Pittsburgh, 1974, pp. 1379-1385.

3. Strahle, W. C., and Shivashankara, B. N., "Combustion Generated Noise in Gas Turbine Combustors," Journal of Engineering for Power, Vol. 98, No. 2, April 1976, pp. 242-246.

4. Saber, A. J., Johnston, M. D., Caveny, L. H., Summerfield, M., and Koury, J., "Acoustic Emissions from Burning Solid Propellant Strands," 11th JANNAF Combustion Meeting, CPIA Publication No. 261, December 1974, pp. 409-428.

5. Caveny, L. H., Saber, A. J., and Summerfield, M., "Propellant Combustion and Burning Rate Uniformity Identified by Ultrasonic Acoustic Emissions," J. Spacecraft and Rockets, Vol. 14, No. 7, July 1977, pp. 434-437.

6. Craig, J. I., Strahle, W. C., and Palfrey, J., "Audible and Ultrasonic Acoustic Emissions from Composite Solid Propellants," AFOSR-75-2805, July 1975.

7. Morse, P. M. and Ingard, K. U., Theoretical Acoustics, Mc-Graw Hill, New York, 1964, Chapter 9.

8. Bell, W. A., Craig, J. I., and Strahle, W. C., "Study of Unsteady Combustion of Heterogeneous Solid Propellants by Analysis of Acoustic Emissions," AIAA Paper No. 77-15, Presented at the 15th Aerospace Sciences Meeting, Los Angeles, CA, January 1977.

9. Acoustic Emission, American Society of Testing and Materials, Special
   Technical Publication, STP-505, Phila., 1972.

10. Dunegan, H. L., and Harris, D. O., "Acoustic Emission Technique,"
    Experimental Techniques in Fracture Mechanics, ed. A. S. Kobayashi,
    SESA Monograph No. 1, Iowa State Univ. Press, p. 38, 1973.

VIII. <u>Tables</u>

Table 1. Physical Properties of the Propellants Tested

Specimen	R-45M	AP Size	AP %	Al	Dioetyl dipate	Indopol	IPDI	Catalysts
MC-170	9.31%	200 μ 14 μ 6 μ	26.8 20.4 20.8	20% 5 μ		2%	0.69%	
MC-172	9.31%	200 μ 14 μ 6 μ	26.8 20.4 20.8	20% 5 μ AFCAM		2%	0.69%	
MC-173	9.31%	200 μ 14 μ 6 μ	26.8 20.4 20.8	20% 5 μ	2%		0.69%	Fe$_2$O$_3$ 2%
MC-179	9.31%	200 μ 14 μ 6 μ	26.8 20.4 20.8	20% 5 μ	2%		0.69%	Copper fluoride 2%
MC-174	10.24%	6 μ 0.5 μ	26 40	20% 5 μ		3%	0.76%	
MC-175	10.24%	6 μ 0.5 μ	26 40	20% 5 μ AFCAM		3%	0.76%	
MC-177	9.31%	400 μ 200 μ 50 μ	44 18 6	20% 5 μ		2%	0.69%	
MC-178	9.31%	400 μ 200 μ 50 μ	44 18 6	20% 5 μ AFCAM		2%	0.69%	

Table 1. Physical Properties of the Propellants Tested (Cont'd)

Specimen	R-45M	AP Size	%	Al
NT-2	20%	200 μ	80	0%
NT-3	20%	90 μ	80	0%
NT-4	20%	50 μ	80	0%
T-273	15%	273 μ	85	0%
T-81	16.9%	81 μ	83.1	0%
T-48	30%	48 μ	70	0%

Table 2. Burn Rates, Combustion Efficiency, and Half-Power Frequency for the Propellants Tested over the Range of Frequencies from 40 to 1000 Hertz.

MC SERIES

Specimen	Percentage of Binder	Chamber Pressure (ATM)	Tube Speed of Sound (Relative)	AP Diameter (Microns)	Burn Rate (in/sec)	Half-Power Frequency (Hertz)	$P/(\dot{m}\,r^2)$ (Dimensionless)
MC-170	12	20	1	83	.432	237	.241
MC-170	12	20	1	83	.360	153	.947
MC-172	12	20	1	83	.416	223	.174
MC-172	12	20	1	83	.424	236	.0067
MC-173	12	20	1	83	.620	211	.0746
MC-173	12	20	1	83	.768	218	.308
MC-174	14	20	1	2.4	.936	400	.0111
MC-174	14	20	1	2.4	.597	222	.105
MC-175	14	20	1	2.4	.752	310	.121
MC-175	14	20	1	2.4	.920	214	.0591
MC-177	12	20	1	316	.176	211	.383
MC-177	12	15	1	316	.178	220	.270
MC-177	12	5	1	316	.123	164	9.75
MC-177	12	10	1	316	.153	359	1.28
MC-177	12	20	1	316	.212	293	.0987
MC-177	12	25	1	316	.217	211	.0839
MC-177	12	30	1	316	.241	183	.0622
MC-178	12	20	1	316	.237	322	.206
MC-179	12	20	1	83	1.37	-	-
MC-179	12	20	1	83	.677	361	.273

Table 2. Burn Rates, Combustion Efficiency, and Half-Power Frequency for the Propellants Tested over the Range of Frequencies from 40 to 1000 Hertz.

NT SERIES

Specimen	Percentage of Binder	Chamber Pressure (ATM)	Tube Speed of Sound (Relative)	AP Diameter (Microns)	Burn Rate (in/sec)	Half-Power Frequency (Hertz)	$P/(\dot{m} r^2)$ (Dimensionless)
NT-2	20	20	1	200	.200	217	.481
NT-2	20	20	1	200	.221	222	.081
NT-2	20	20	2.88	200	.223	151	.0552
NT-2	20	5	1	200	.0974	282	5.18
NT-2	20	10	1	200	.140	405	1.05
NT-2	20	15	1	200	.171	321	.274
NT-2	20	20	1	200	.202	264	.150
NT-2	20	25	1	200	.217	265	.0899
NT-2	20	30	1	200	.258	176	.0435
NT-2	20	20	1	200	.222	296	.223
NT-3	20	20	1	90	.358	326	.0181
NT-3	20	20	2.88	90	.297	129	.0325
NT-3	20	20	2.88	90	.310	101	.0127
NT-3	20	20	1	90	.290	364	.0800
NT-4	20	20	2.88	50	.331	335	.0233
NT-4	20	20	2.88	50	.331	224	.0249
NT-4	20	20	2.88	50	.358	84	.0255
NT-4	20	15	2.88	50	.308	54	.0560
NT-4	20	30	2.88	50	.441	147	.00598
NT-4	20	23	2.88	50	.378	282	.0209

Table 2. Burn Rates, Combustion Efficiency, and Half-Power Frequency for the Propellants Tested over the Range of Frequencies from 40 to 1000 Hertz.

T SERIES

Specimen	Percentage of Binder	Chamber Pressure (ATM)	Tube Speed of Sound (Relative)	AP Diameter (Microns)	Burn Rate (in/sec)	Half-Power Frequency (Hertz)	$P/(\dot{m}\,r^2)$ (Dimensionless)
T-81	16.9	15	1	81	.298	312	.369
T-81	16.9	10	1	81	.244	439	1.05
T-81	16.9	30	1	81	.476	307	.0558
T-81	16.9	20	1	81	.357	308	.674
T-81	16.9	5	1	81	.162	249	5.52
T-81	16.9	25	1	81	.408	312	.102
T-81	16.9	20	1	81	.394	347	.296
T-273	15	20	1	273	.325	200	.0775
T-48	30	20	1	48	.148	435	.435
T-48	30	20	1	48	.150	395	.451
T-48	30	20	1	48	.152	405	.329
T-273	15	20	1	273	.267	283	.139
T-48	30	20	2.88	48	.158	498	.0683
T-273	15	20	2.88	273	.294	421	.0736

Table 3. Results of the Regression Analysis
Using the Data from Table 2.

Variable	Definition
x_1	Percentage of binder
x_2	Chamber pressure
x_3	Chamber sound speed
x_4	AP particle diameter
x_5	Burn rate
x_6	Dependent variable - $\omega_{\frac{1}{2}}$ or η

$$\omega_{\frac{1}{2}}, \eta \sim (x_1)^a (x_2)^b (x_3)^c (x_4)^d (x_5)^e$$

| Cross Correlation Coefficient | Frequency Range | | | |
	0-1000 Hz		0-10 kHz	
	$\omega_{\frac{1}{2}}$	η	$\omega_{\frac{1}{2}}$	η
R_{16}	.154	-.097	.340	.082
R_{26}	-.054	-.742	.198	-.622
R_{36}	-.409	-.510	.855	-.643
R_{46}	-.050	.288	-.047	.431
R_{56}	-.148	-.600	.123	-.717
a	.38	-.50	.14	2.9
b	.09	-1.9	-.06	-2.8
c	-.49	-1.4	.24	-4.1
d	-.07	.16	.04	.38
e	-.19	-1.5	.13	-1.6

IX. <u>Figures</u>
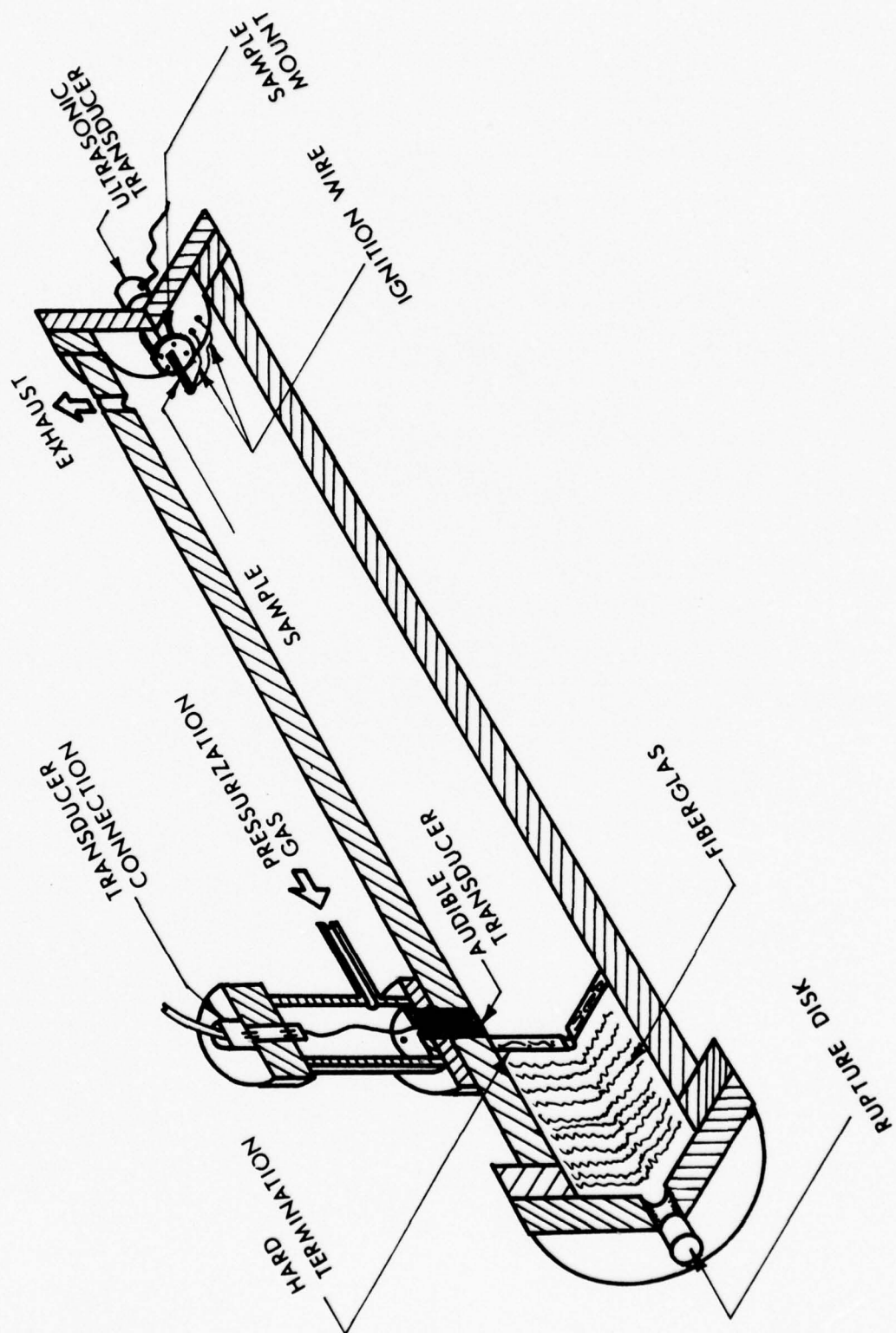
FIGURE 1. SCHEMATIC OF DEFLAGRATION TUBE.
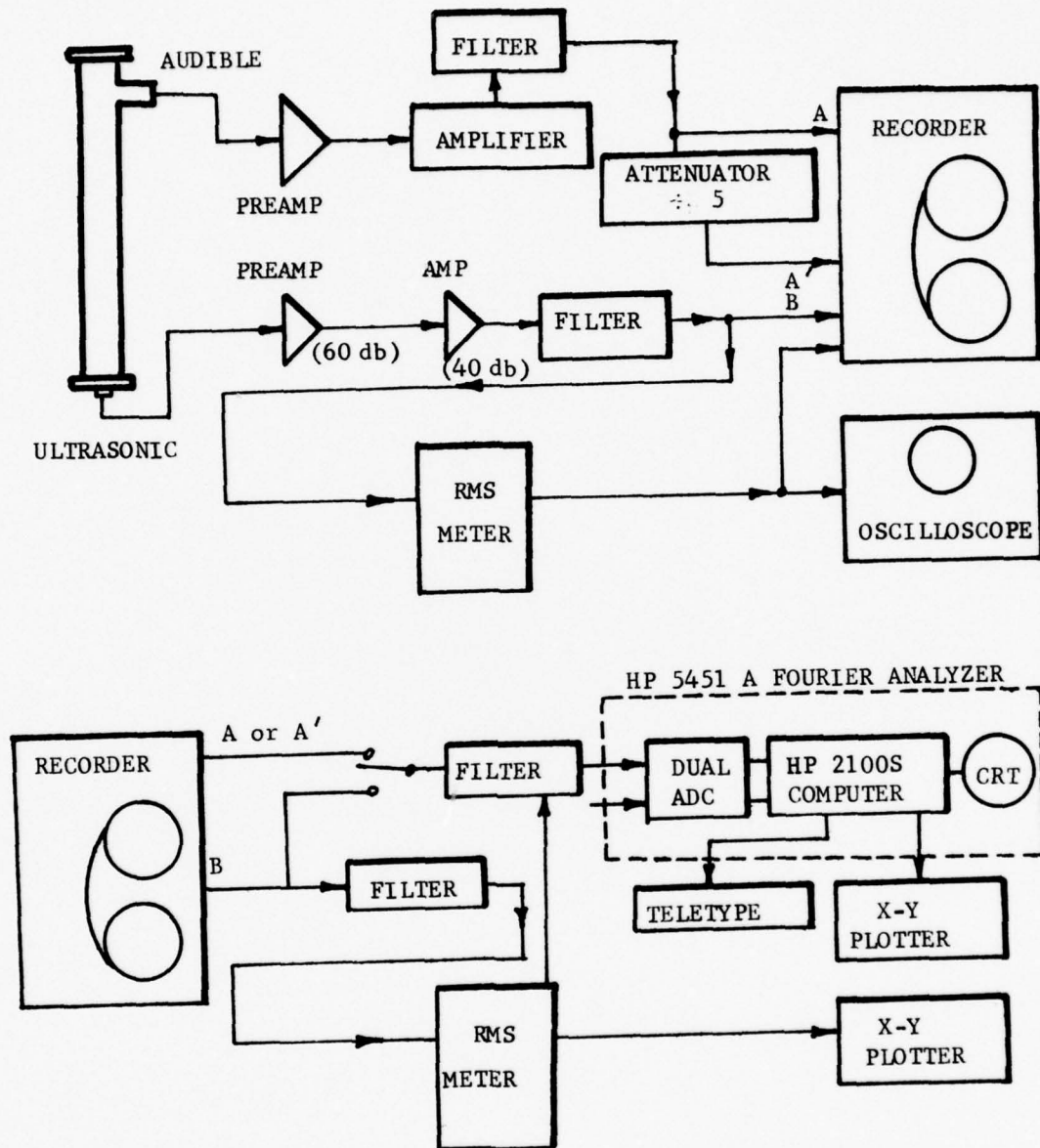
FIGURE 2. DATA ACQUISITION AND ANALYSIS SCHEMATIC
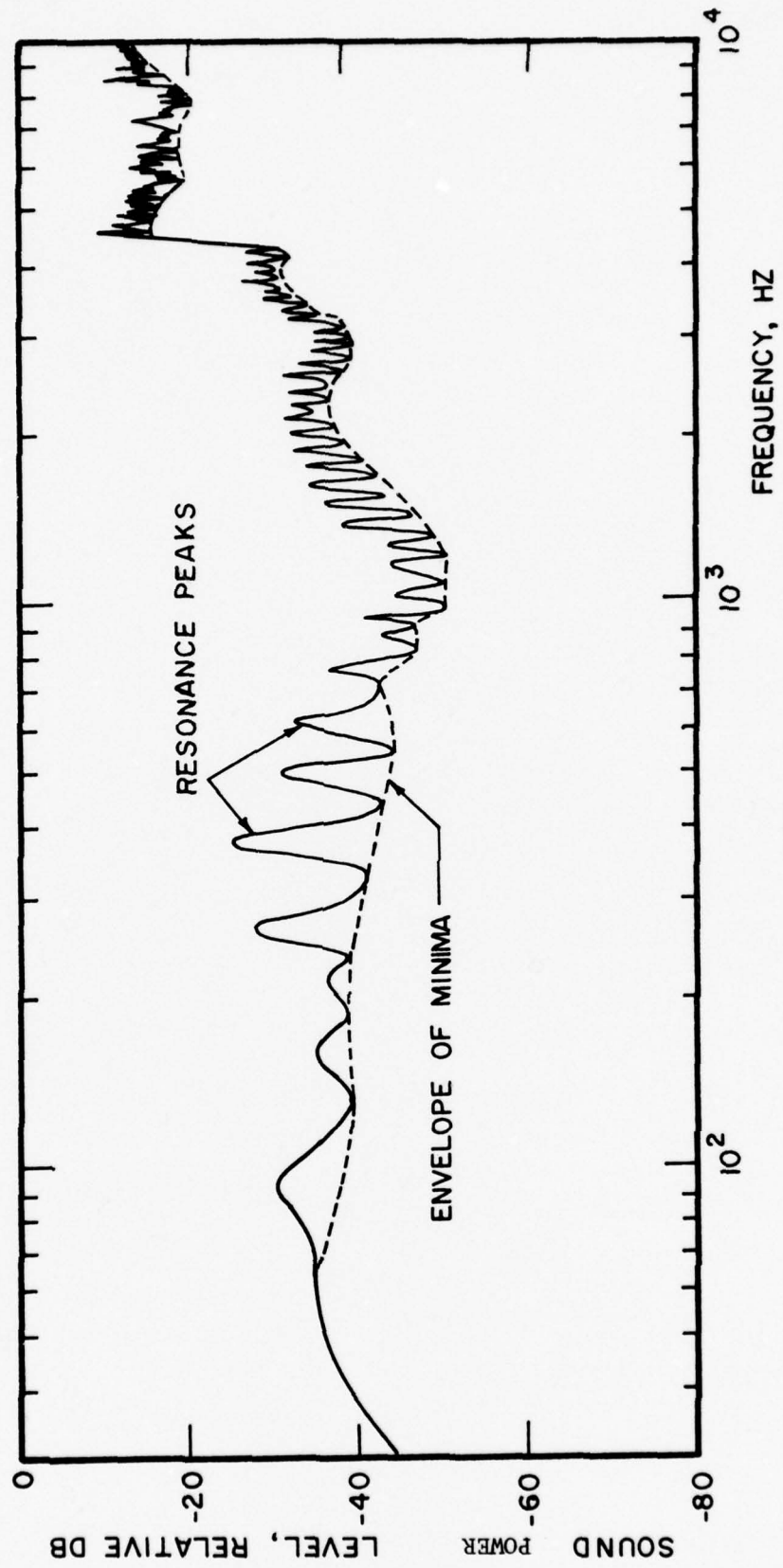
FIGURE 3. RAW SPECTRUM FOR NT-2 BURNING IN NITROGEN AT 300 PSIA.
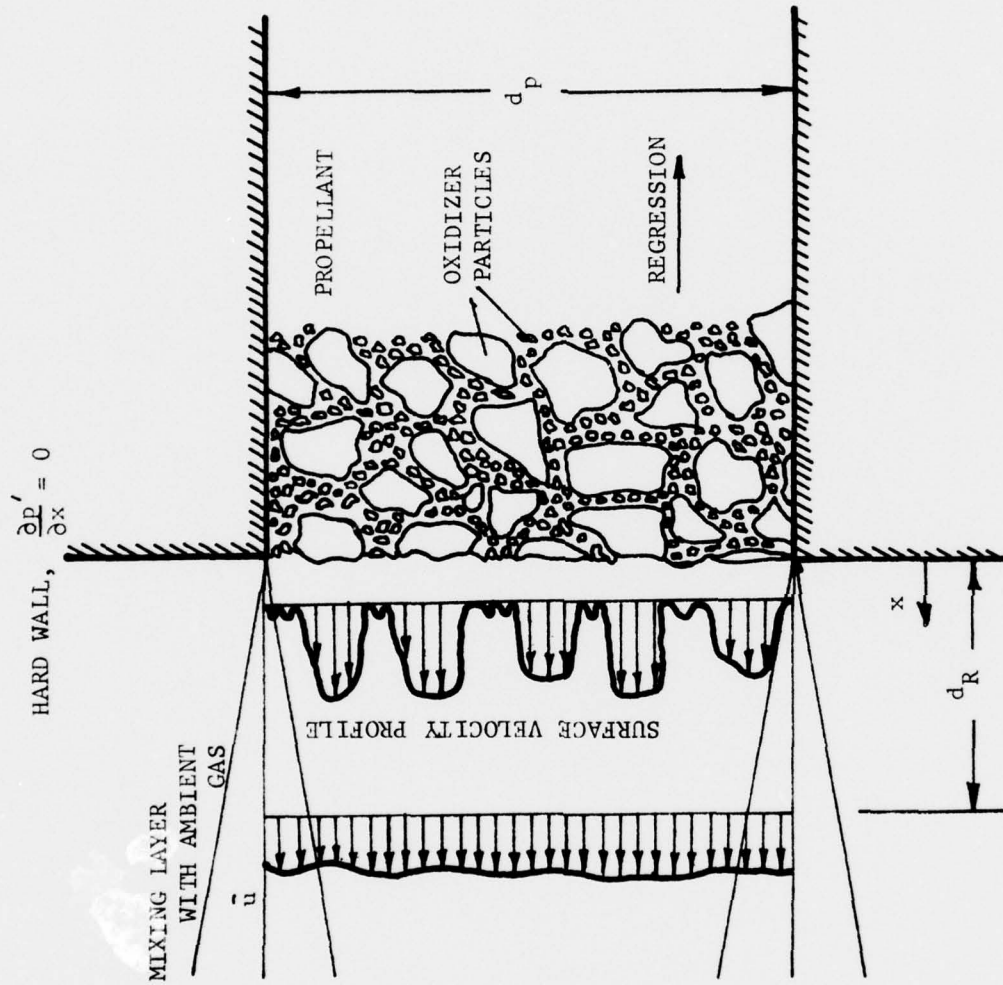
FIGURE 4. DIAGRAM OF THE COMBUSTION REACTION ZONE

48
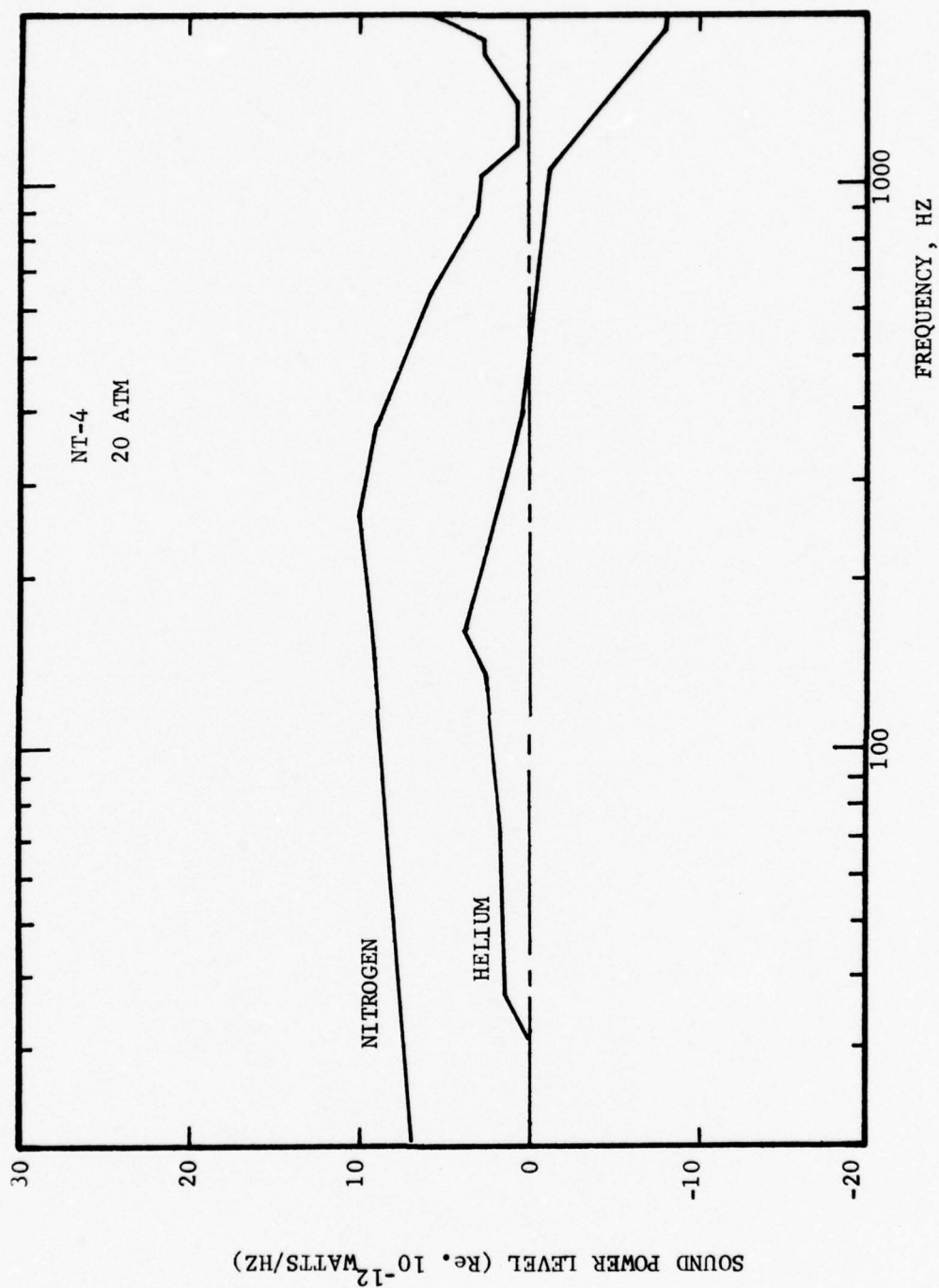
FIGURE 5. EFFECT OF CHAMBER GAS ON DEDUCED FREE
FIELD POWER SPECTRUM
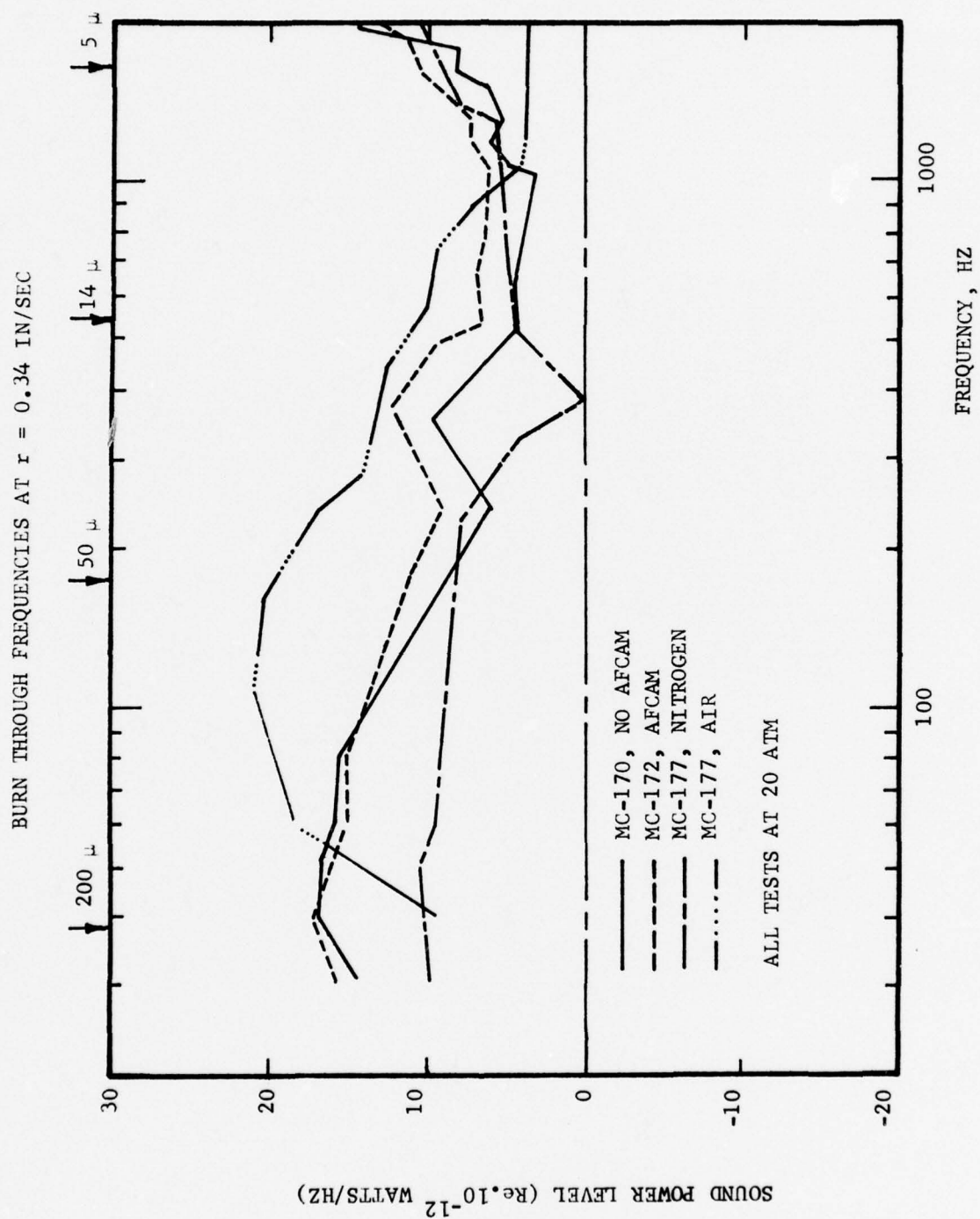
FIGURE 6. EFFECTS OF AP PARTICLE SIZE, AFCAM TREATMENT, AND CHAMBER GAS ON DEDUCED FREE FIELD SPECTRA.
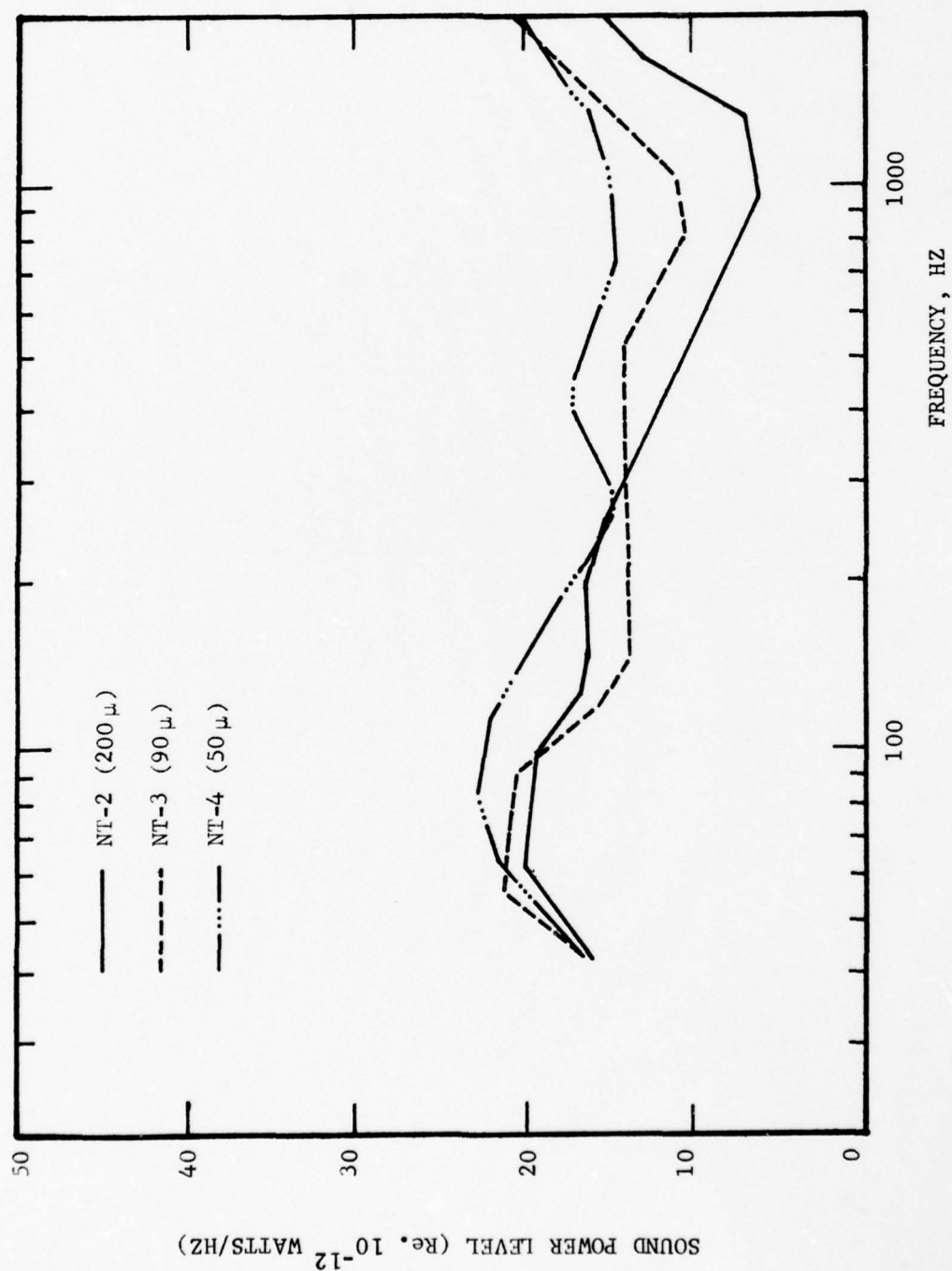
FIGURE 7. COMPARISON OF DEDUCED FREE FIELD SPECTRA FOR NONALUMINIZED PROPELLANTS
BURNED AT 300 PSIA IN NITROGEN
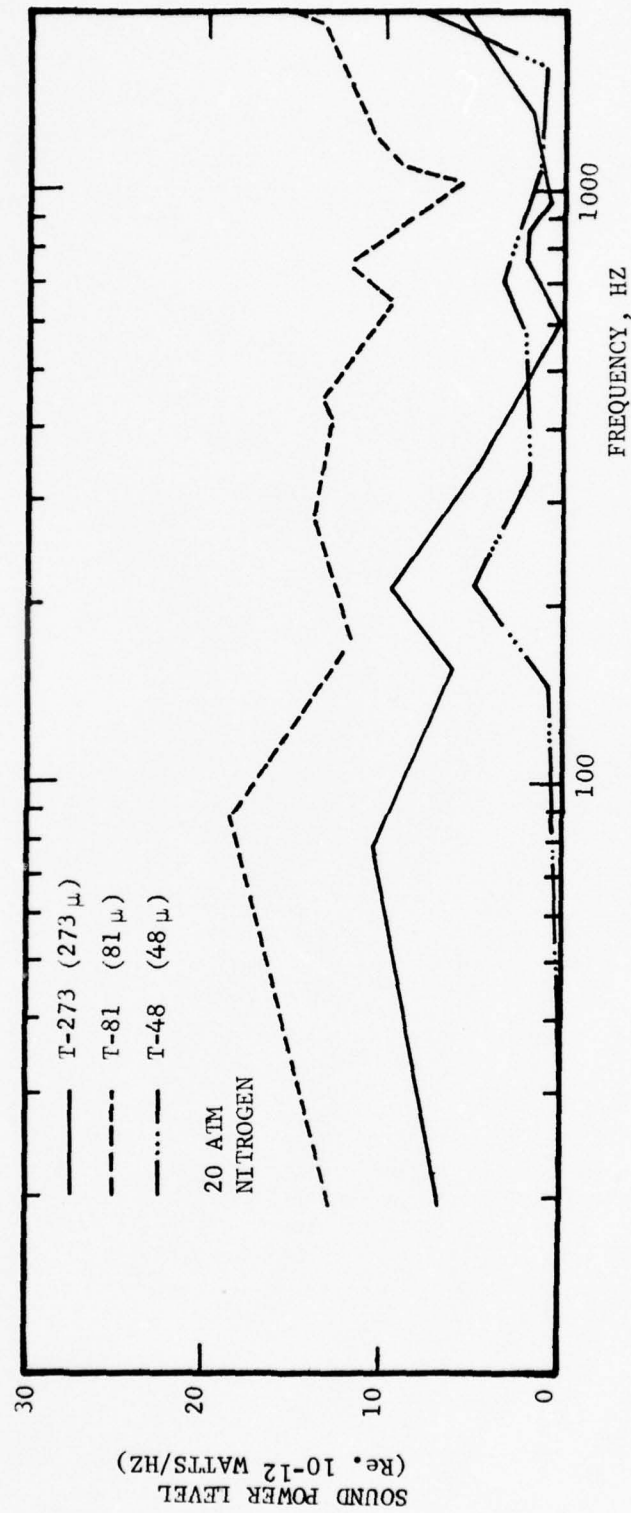
FIGURE 8. EFFECT OF PARTICLE SIZE ON DEDUCED FREE FIELD SPECTRA FOR NONALUMINIZED PROPELLANTS, T-SERIES
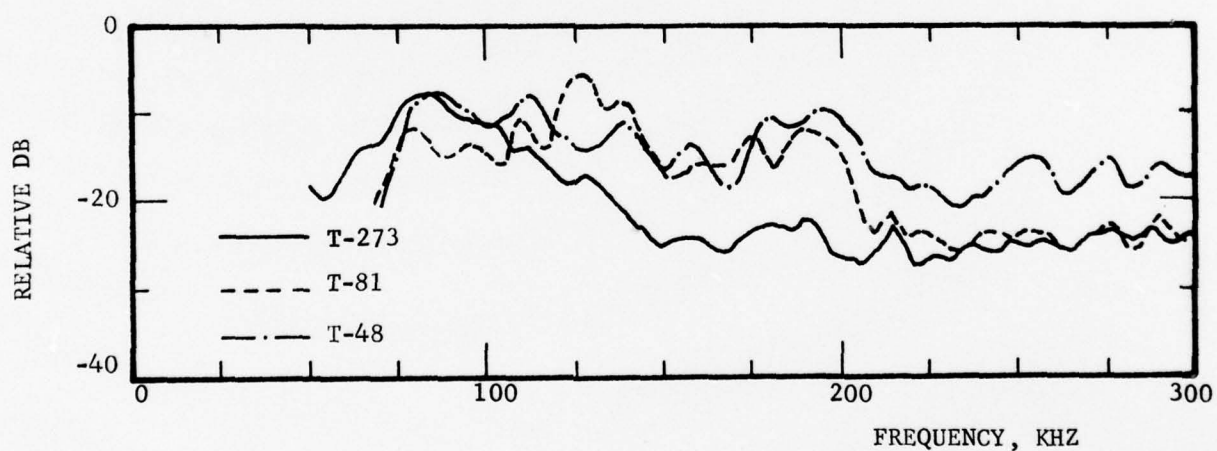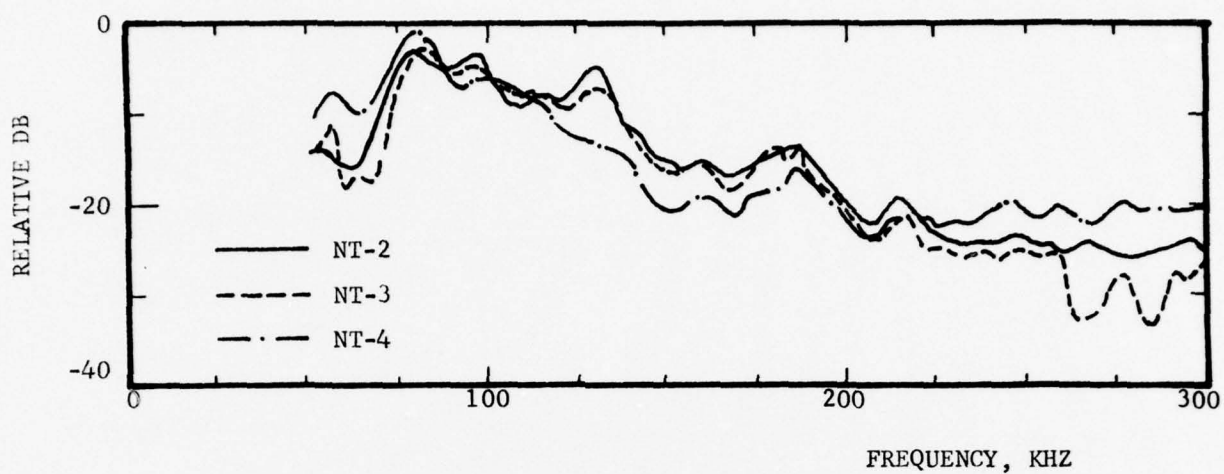
FIGURE 9. EFFECT OF AP PARTICLE SIZE ON THE ACOUSTIC EMISSION SPECTRA FOR THE NONALUMINIZED PROPELLANTS BURNED IN NITROGEN AT 300 PSIA.
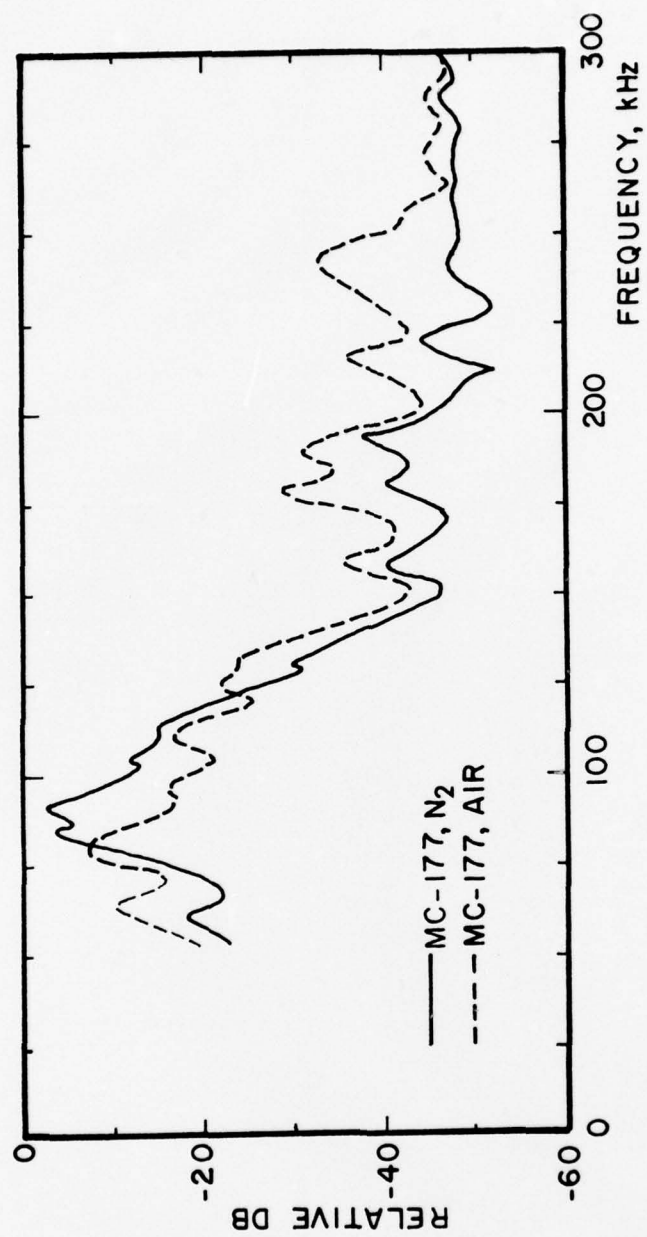
FIGURE 10. EFFECT OF PRESSURIZATION GAS ON THE ULTRASONIC SPECTRA OF MC-177 AT 300 PSIA
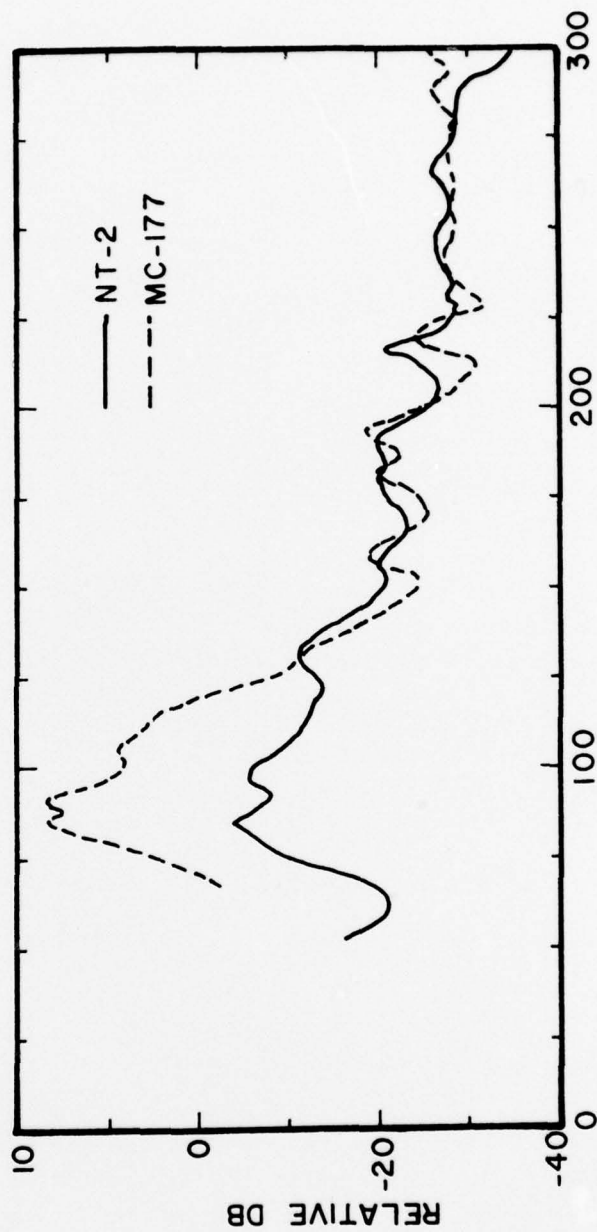
FIGURE 11. EFFECT OF ALUMINUM ADDITION ON THE ULTRASONIC SPECTRA
AT 300 PSIA BURNED IN NITROGEN.
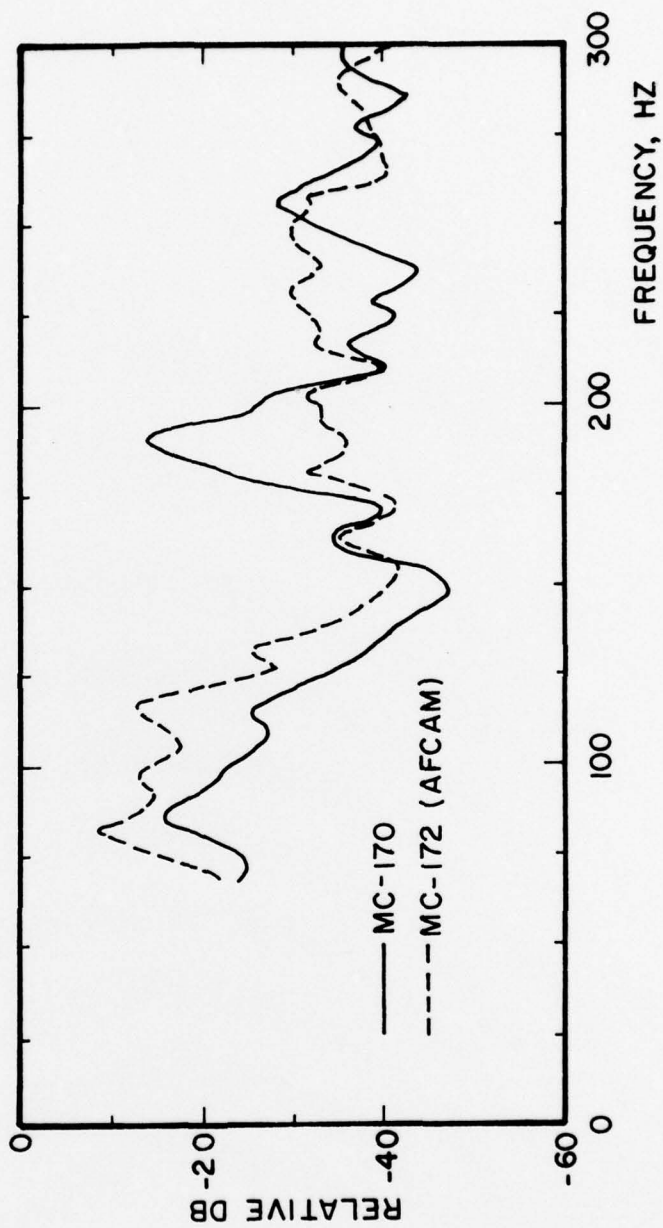
FIGURE 12. EFFECT OF AFCAM COATING OF THE
ALUMINUM PARTICLES AT 300 PSIA
IN NITROGEN.
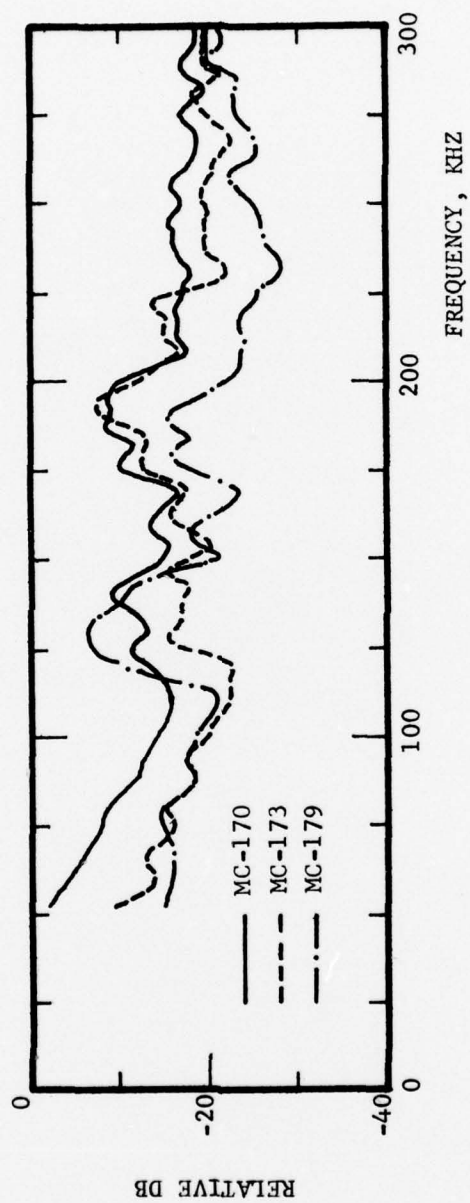
FIGURE 13. EFFECT OF CATALYSTS ON THE SOUND POWER SPECTRA FOR THE ACOUSTIC EMISSIONS.
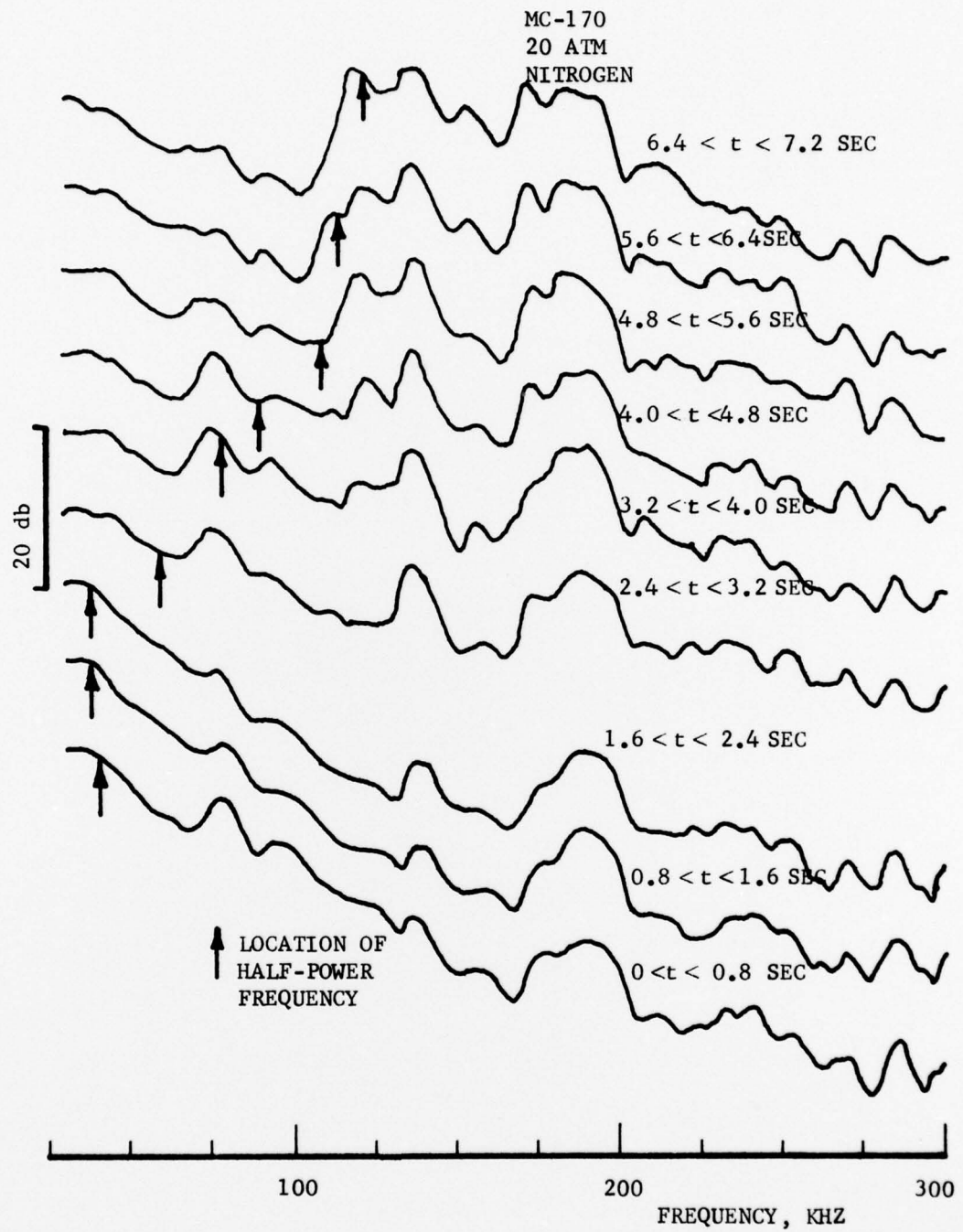
FIGURE 14. NONSTATIONARITY OF THE ACOUSTIC EMISSIONS DURING DEFLAGRA-
TION AS TIME INCREASES.
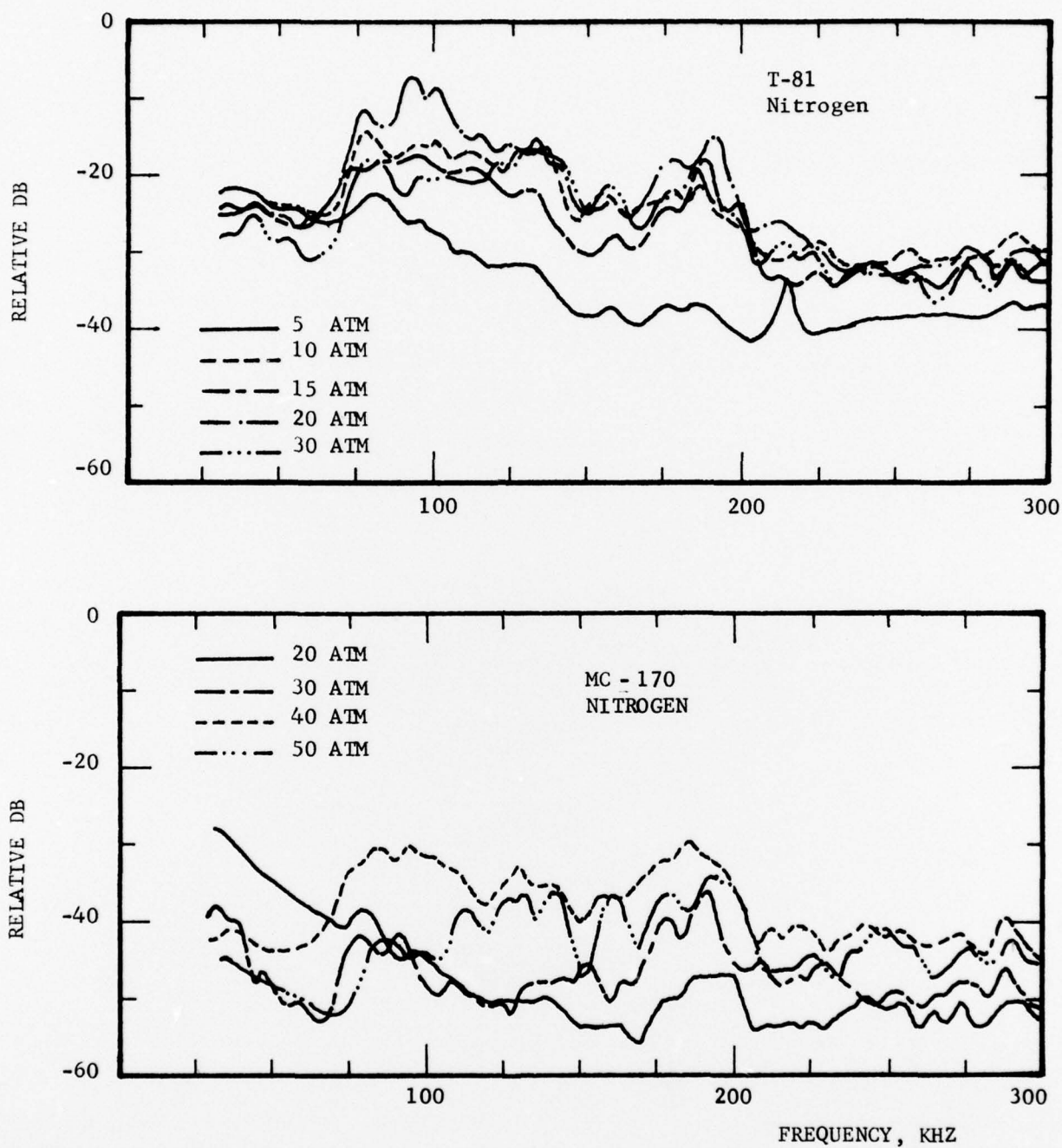
FIGURE 15. EFFECT OF CHAMBER PRESSURE ON THE ACOUSTIC EMISSION SOUND POWER SPECTRA FOR NONALUMINIZED AND ALUMINIZED PROPELLANTS.
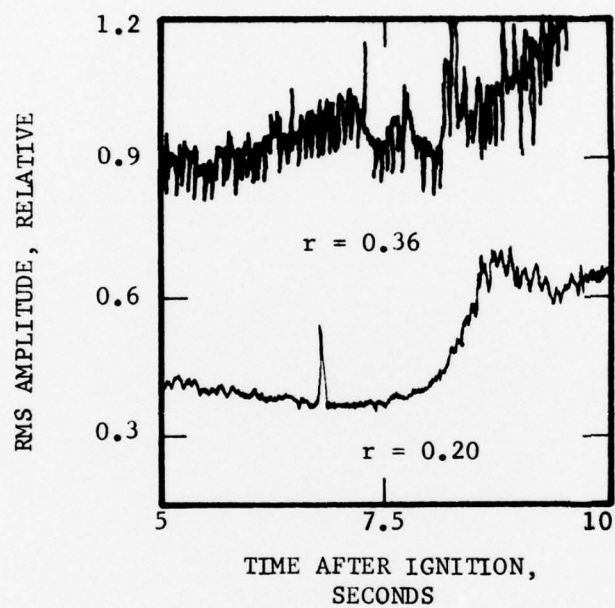
FIGURE 16. INCREASE IN ACOUSTIC EMISSIONS
WHICH ACCOMPANIES AN ABNORMALLY
HIGH BURN RATE FOR NT-2 at 20ATM
IN NITROGEN.
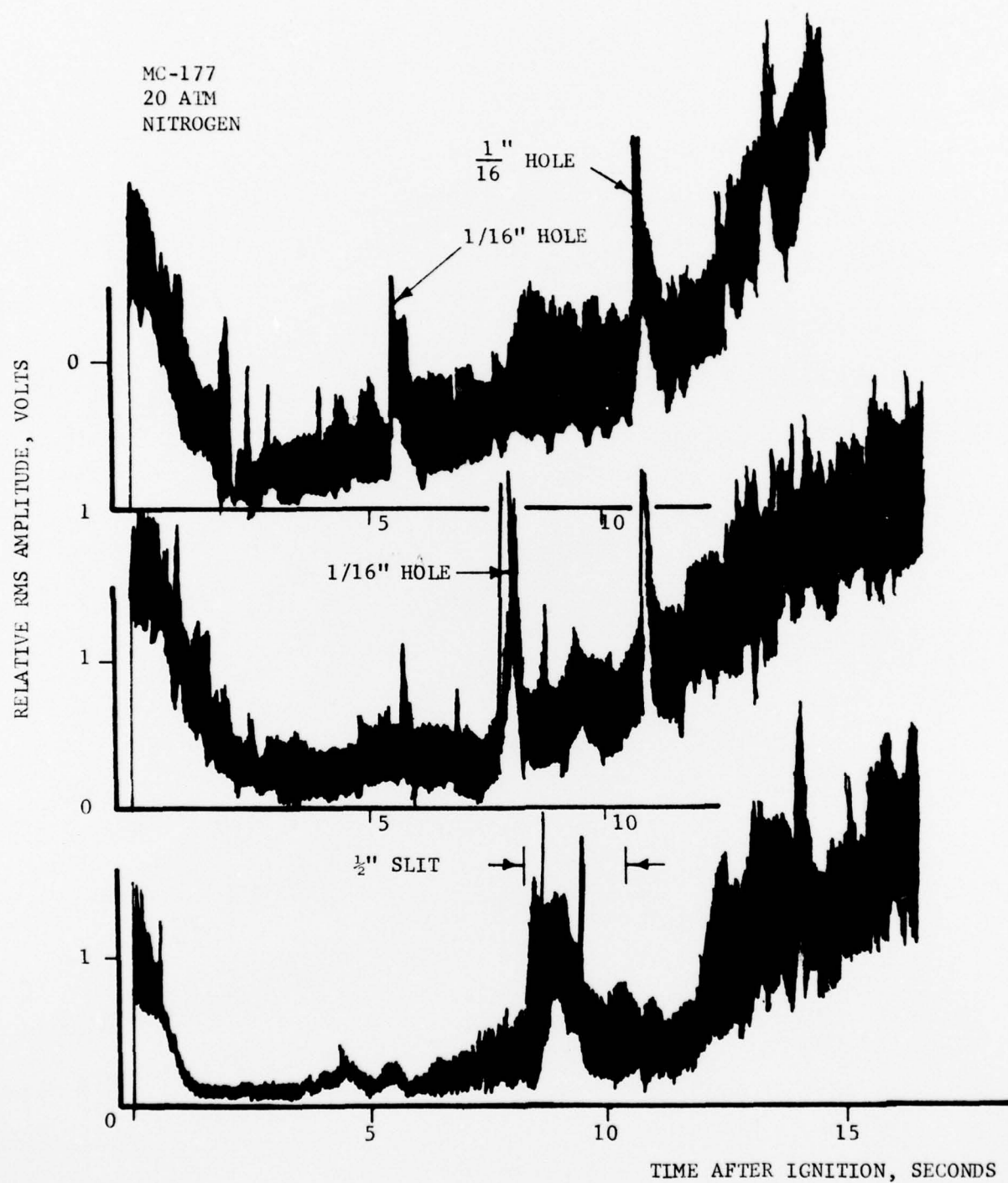
FIGURE 17. EFFECT OF IMPERFECTIONS SYSTEMATICALLY INTRODUCED IN THE
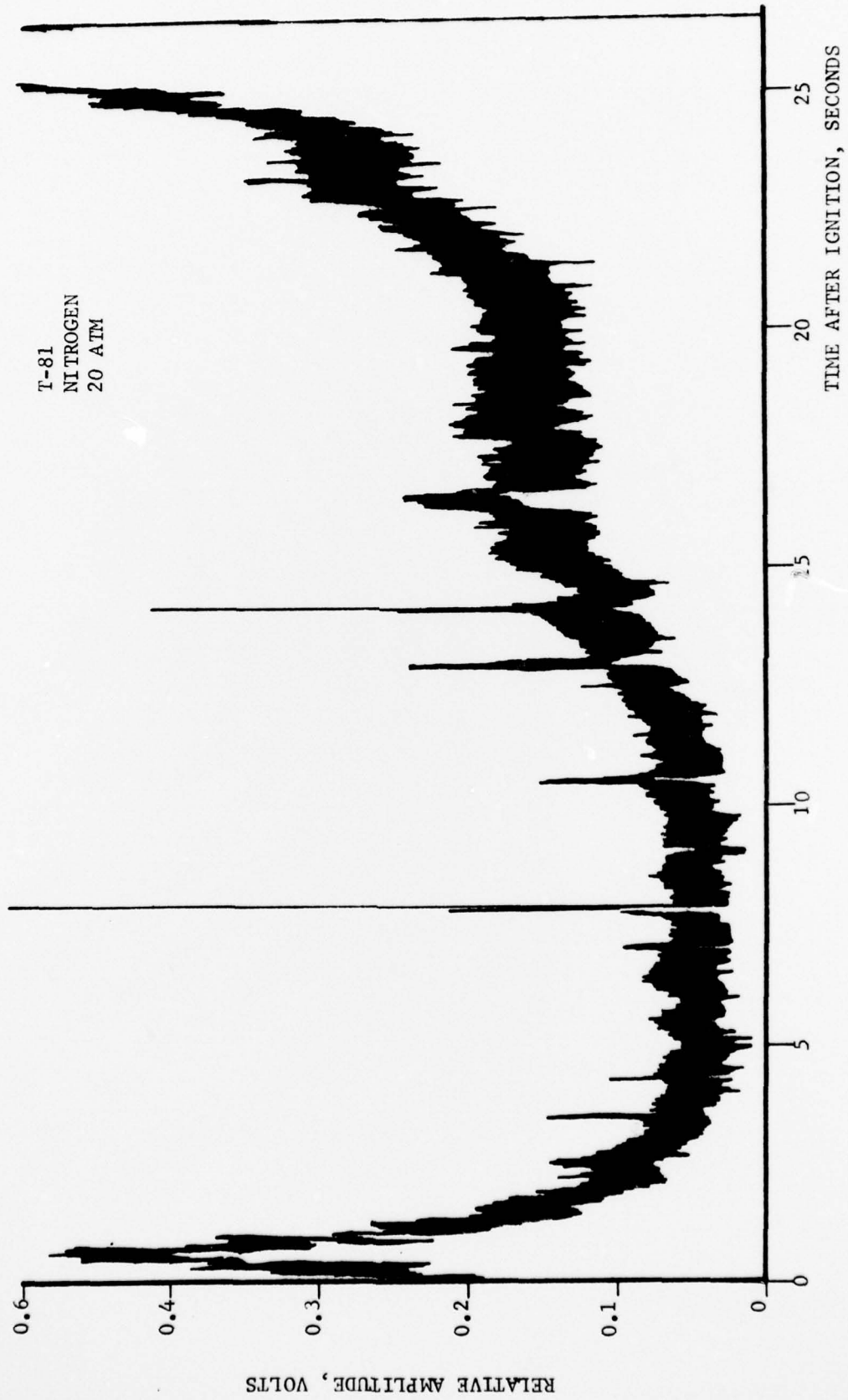PROPELLANT SAMPLE ON THE RMS LEVELS OF THE ACOUSTIC EMISSIONS.

FIGURE 18. ANOMALOUS BEHAVIOR OF THE RMS ACOUSTIC EMISSION LEVELS. THE "SPIKES" ARE PROBABLY CAUSED BY BUBBLES IN THE PROPELLANT INTRODUCED DURING PREPARATION.
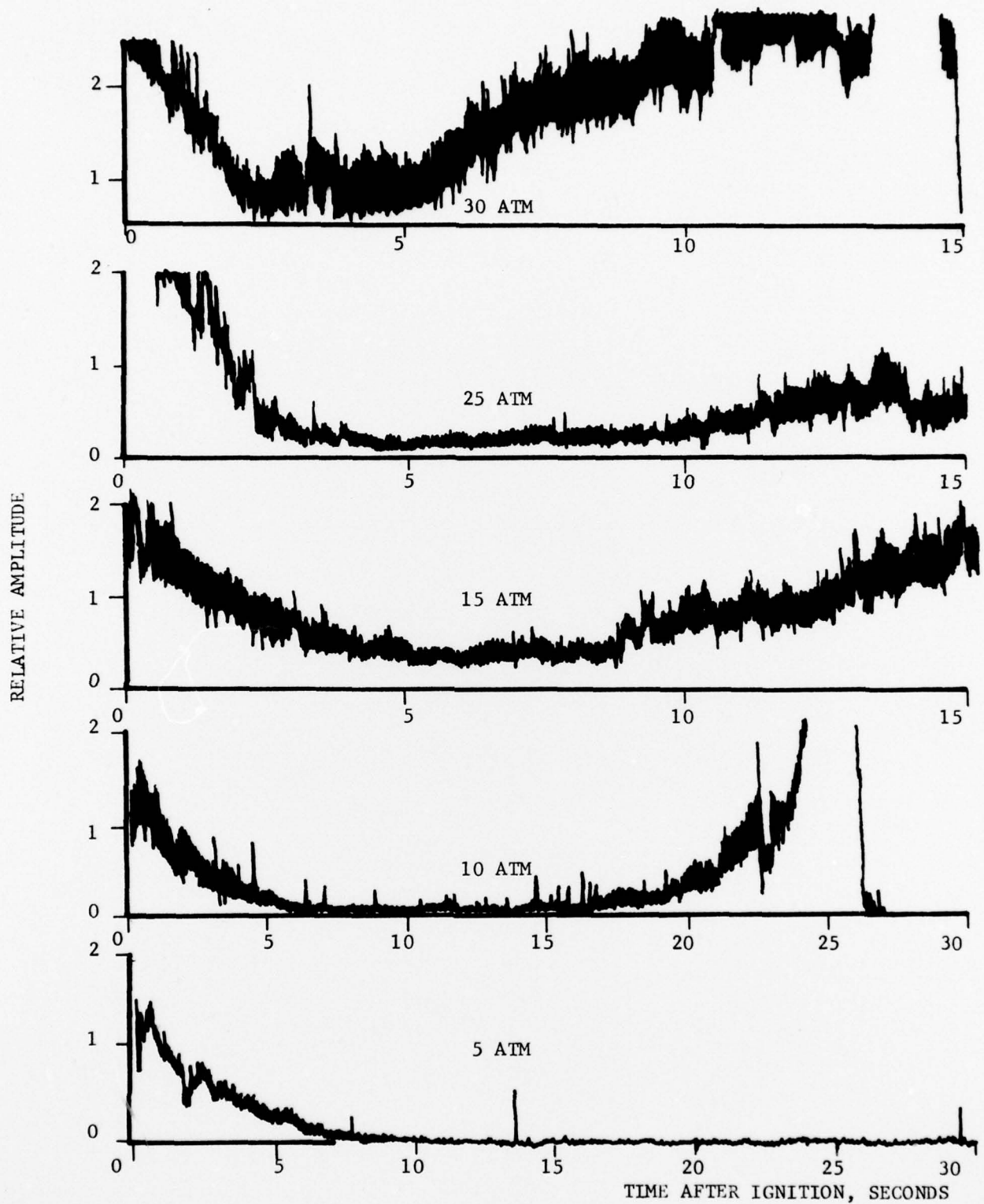
FIGURE 19. EFFECT OF CHAMBER PRESSURE ON THE RMS ACOUSTIC EMISSION
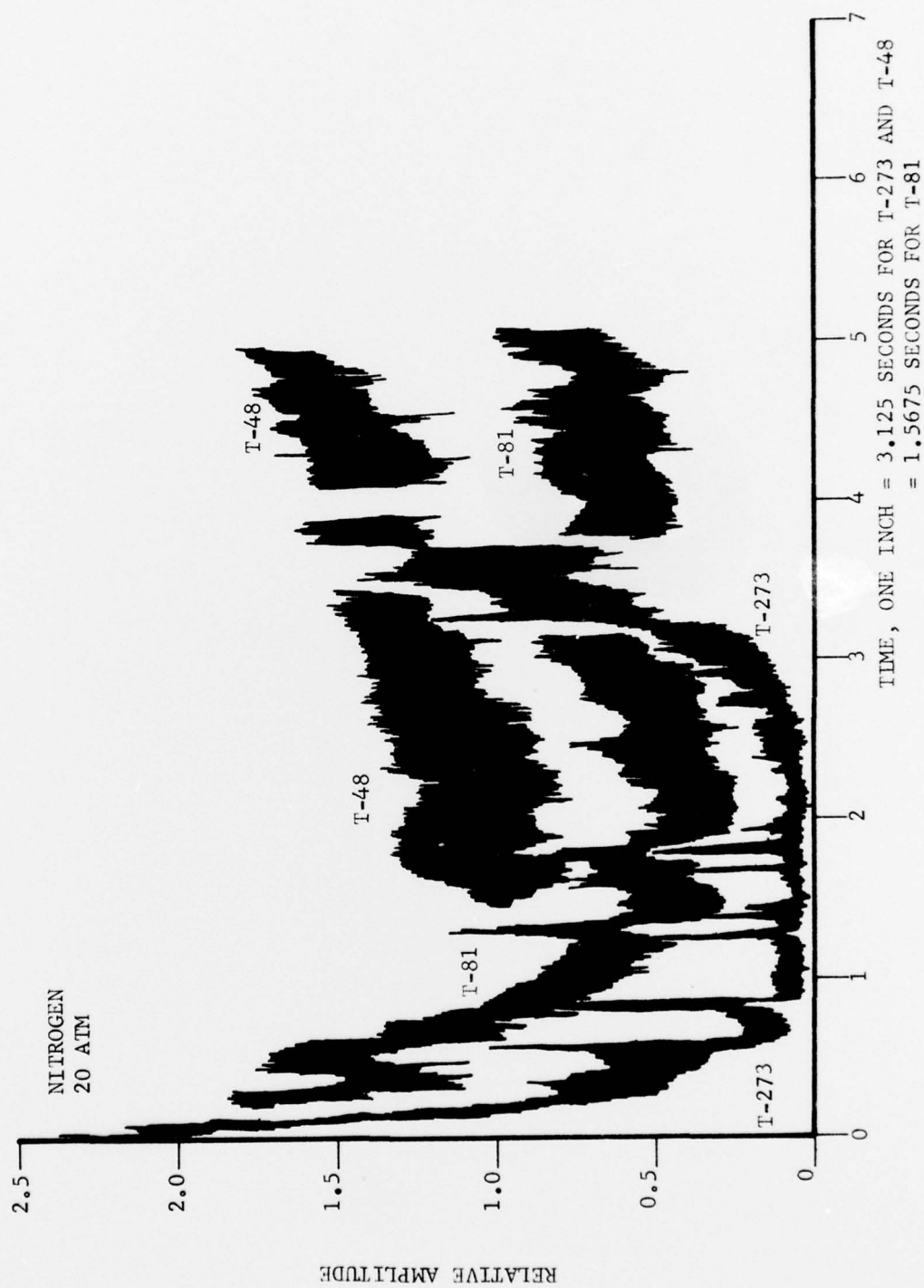LEVELS FOR NT-2 IN NITROGEN.

FIGURE 20. EFFECT OF PARTICLE SIZE ON THE RMS ACOUSTIC EMISSION LEVELS FOR A NON-ALUMINIZED SERIES OF PROPELLANTS.
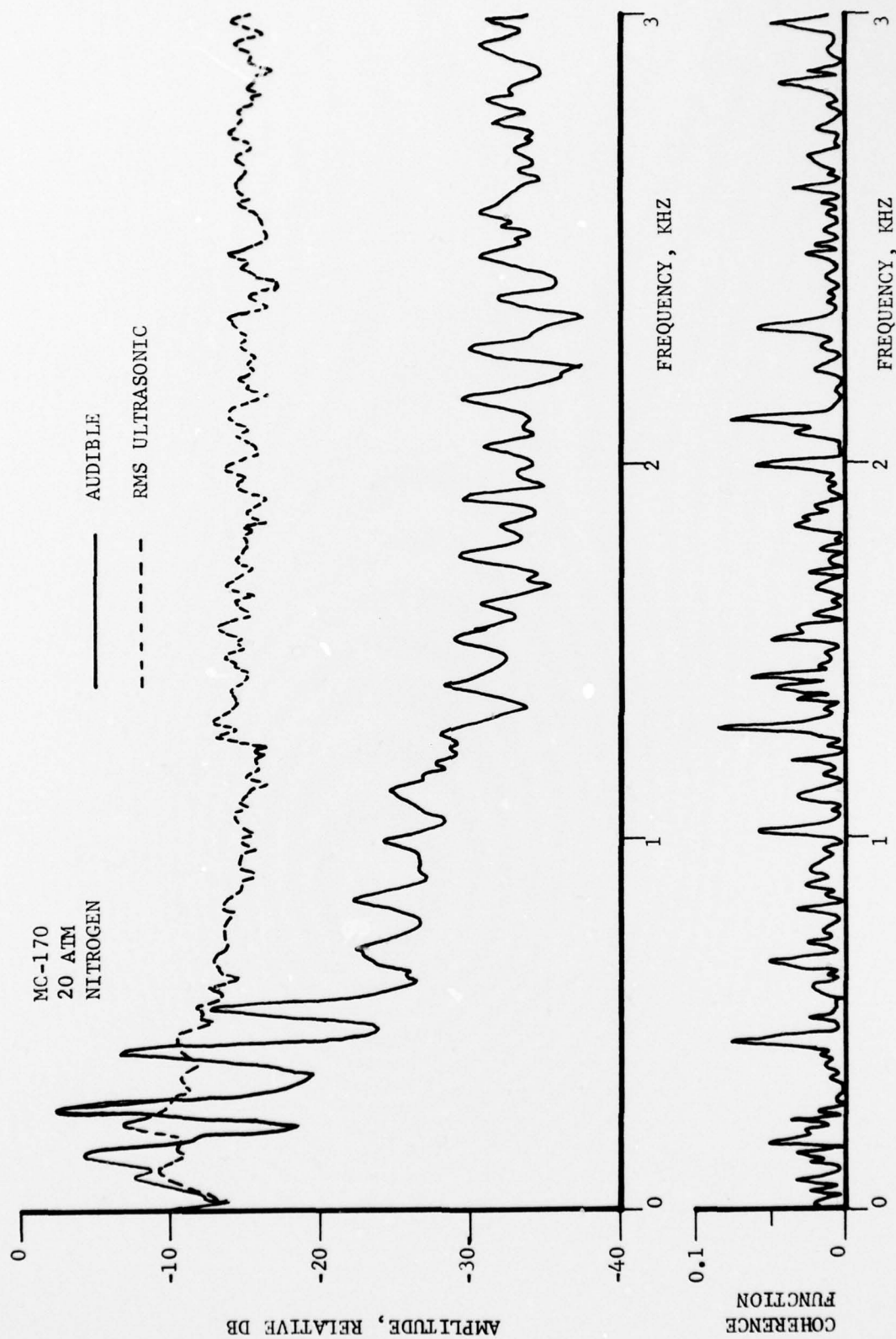
FIGURE 21. CORRELATION OF THE RMS ACOUSTIC EMISSION SIGNAL WITH THE AUDIBLE SIGNAL FOR AN ALUMINIZED PROPELLANT.

REPORT DOCUMENTATION PAGE

READ INSTRUCTIONS
BEFORE COMPLETING FORM

1. REPORT NUMBER AFOSR-TR- **78**- 0 0 0 9	2. GOVT ACCESSION NO.	3. RECIPIENT'S CATALOG NUMBER

4. TITLE (and Subtitle)

AUDIBLE AND ULTRASONIC ACOUSTIC EMISSIONS
FROM COMPOSITE SOLID PROPELLANTS

5. TYPE OF REPORT & PERIOD COVERED

FINAL

Oct 76 – Sep 77

6. PERFORMING ORG. REPORT NUMBER

7. AUTHOR(s)

WILLIAM A BELL
JAMES I CRAIG
WARREN C STRAHLE

8. CONTRACT OR GRANT NUMBER(s)

AFOSR 75-2805

9. PERFORMING ORGANIZATION NAME AND ADDRESS

GEORGIA INSTITUTE OF TECHNOLOGY
SCHOOL OF AEROSPACE ENGINEERING
ATLANTA, GEORGIA 30332

10. PROGRAM ELEMENT, PROJECT, TASK AREA & WORK UNIT NUMBERS

2308A1

61102F

11. CONTROLLING OFFICE NAME AND ADDRESS

AIR FORCE OFFICE OF SCIENTIFIC RESEARCH/NA
BLDG 410
BOLLING AIR FORCE BASE, D C 20332

12. REPORT DATE

Sep 77

13. NUMBER OF PAGES

67

14. MONITORING AGENCY NAME & ADDRESS(if different from Controlling Office)

15. SECURITY CLASS. (of this report)

UNCLASSIFIED

15a. DECLASSIFICATION/DOWNGRADING SCHEDULE

16. DISTRIBUTION STATEMENT (of this Report)

Approved for public release; distribution unlimited.

17. DISTRIBUTION STATEMENT (of the abstract entered in Block 20, if different from Report)

18. SUPPLEMENTARY NOTES

19. KEY WORDS (Continue on reverse side if necessary and identify by block number)

ULTRASONICS
NOISE
SOLID PROPELLANT COMBUSTION
ACOUSTIC EMISSIONS

20. ABSTRACT (Continue on reverse side if necessary and identify by block number)

The audible and ultrasonic acoustic emissions from deflagrating composite solid propellants were monitored and analyzed to evaluate their potential use as diagnostics of the combustion and as a means for the study of fundamental burning processes. A family of composite HTPB-AP propellants were tested which include a range of AP particle sizes, aluminized and nonaluminized formulations, the effect of the addition of a catalyst, and the presence of an AFCAM aluminum coating. For the audible emissions, the frequency behavior in the 0–10 kHz range can be explained by assuming the gas phase reaction time primarily controls the oscillating frequency. The combustion noise efficiency cannot

DD FORM 1 JAN 73 **1473** EDITION OF 1 NOV 65 IS OBSOLETE

be explained by the theories put forth, so the physical makeup of the noise source is presently unknown.   Analysis of the ultrasonic emission spectra indicates that there are no distinct spectral features which can be used to identify a particular propellant by its acoustic signature.   The rms emission levels, however, can be used as a reliable, non-intrusive means for detecting flaws in the propellant, identifying bad burns, and measuring burn rates.   The overall level increases with increasing burn rate and chamber pressure and decreasing particle size.

UNCLASSIFIED